arXiv:astro-ph/0210624v1 29 Oct 2002

Carbon-Oxygen White Dwarfs Accreting CO-Rich Matter I: A Comparison Between Rotating and Non-Rotating Models

Luciano Piersanti [1]

Dipartimento di Fisica dell'Università degli Studi di Napoli "Federico II", Mostra d'Oltremare, pad. 20, 80125, Napoli, Italy; piersanti@astrte.te.astro.it

Simona Gagliardi

Osservatorio Astronomico di Teramo, Via M.Maggini 47, 64100 Teramo, Italy; gagliardi@astrte.te.astro.it

Icko Iben Jr.

Astronomy Department, University of Illinois, 1002 W. Green Street, Urbana, IL 61801;icko@astro.uiuc.edu

and

Amedeo Tornambé

Osservatorio Astronomico di Teramo, Via M.Maggini 47, 64100 Teramo, Italy; tornambe@astrte.te.astro.it

[1]Osservatorio Astronomico di Teramo, Via M.Maggini 47, 64100 Teramo, Italy

Received _____; accepted _____

ABSTRACT

We investigate the lifting effect of rotation on the thermal evolution of carbon-oxygen white dwarfs accreting carbon-oxygen-rich matter. We find that rotation induces the cooling of the accreting structure so that the delivered gravitational energy causes a greater expansion with respect to the standard non-rotating case. The increase in the surface radius produces a decrease in the surface value of the critical angular velocity and, therefore, the accreting white dwarf becomes gravitationally unbound (Roche instability). This occurrence is due to an increase in the total angular momentum of the accreting white dwarf and depends critically on the amount of specific angular momentum deposited by the accreted matter. If the specific angular momentum of the accreted matter is equal to that of the outer layers of the accreting structure, the Roche instability occurs well before the accreting white dwarf can attain the physical conditions for carbon burning. If the values of both initial angular velocity and accretion rate are small, we find that the accreting white dwarf undergoes a secular instability when its total mass approaches 1.4 $M_{\odot}$. At this stage, the ratio between the rotational energy and the gravitational binding energy of the white dwarf becomes of the order of 0.1, so that the star must deform by adopting an elliptical shape. In this case, since the angular velocity of the white dwarf is as large as ~ 1 rad s^{-1}, the anisotropic mass distribution induces the loss of rotational energy and angular momentum via gravitational wave radiation. We find that, independent of the braking efficiency, the white dwarf contracts and achieves the physical conditions suitable for explosive carbon burning at the center so that a type Ia supernova event is produced.

Subject headings: stars: accretion, rotation - supernovae: general - white dwarf

1. Introduction

Type Ia Supernovae (SNe Ia) are one of the most powerful tools for determining the rate of expansion and elucidating the geometrical structure of the Universe. They are intrinsically very luminous objects and, provided the empirical relation between the absolute magnitude at maximum light and the rate of decline from maximum (Phillips 1993) proves to be theoretically well founded and universally valid, they may eventually be used as fairly reliable distance indicators. For each observed event, it may then be possible to estimate reliably the luminosity at maximum and, hence, to determine the distance modulus.

Despite the pivotal role of the observed correlation in observational cosmology, a theoretical justification for the correlation does not yet exist. Nevertheless, a Phillips relation which has been constructed from a sample of only nine local ($z < 0.5$) supernovae (SNe) has been used to estimate the distances to many more SNe at much larger z, assuming that no differences at all exist between events produced by different stellar populations in the past.

Finally, from the theoretical point of view, a definitive identification of the progenitor system and an understanding the full nature of the explosion mechanism are still missing. At present it is accepted that SNe Ia are produced by the thermonuclear disruption of a carbon-oxygen (CO) white dwarf (WD) which has attained the Chandrasekhar mass ($M_{\rm Ch}$). Hoyle & Fowler (1960) were the first to examine the nucleosynthetic characteristics of such an explosion, without specifying how the initial configuration comes about. Arnett (1969) demonstrated that, without the mass loss which in real life terminates its evolution, an intermediate mass single star would ultimately develop a CO core of Chandrasekhar mass. We now know that single intermediate mass stars end their nuclear burning evolution with the ejection of their hydrogen-rich envelopes (illuminated for a brief time as planetary nebulae) and evolve into white dwarfs of mass considerably smaller than the Chandrasekhar

mass. The consensus view has become that the progenitors of type Ia supernovae are close binary star systems. The most traditional scenario is the single degenerate (SD) one in which it is assumed that the accreted matter is supplied by a companion which is composed of hydrogen-rich matter (Whelan & Iben 1973). An alternate scenario is the double-degenerate (DD) one which argues that evolutionary paths exist for producing two CO white dwarfs which are close enough to merge in a Hubble time (due to angular momentum loss by gravitational wave radiation) and whose combined mass exceeds $M_{\rm Ch}$. This second scenario, examined by Iben & Tutukov (1984) and by Webbink (1984), has been questioned from time to time. Two main features make the DD scenario attractive: 1) the total absence of hydrogen in the progenitor system and 2) the fact that the more massive WD approaches the critical mass in a very natural way. Yet, in spite of huge observational efforts, only one good candidate SN Ia progenitor has been identified (KPD 0422+5421 - see Koen, Orosz & Wade 1998); in fact, this is the only system yet found the total mass of which is of the order of $M_{\rm Ch}$ and the components of which will merge in less than a Hubble time due to gravitational wave radiation (GWR). Other observed systems with an orbital period short enough for a merger to occur in less than a Hubble time have a total mass which is too small for the system to qualify as a SN Ia progenitor (see Saffer, Livio & Yungelson (1998) and also Livio (2000) for a recent review). Nevertheless, population synthesis estimates suggest that enough massive close binary systems are produced in nature to account for the observed frequency of SNe Ia events (Iben, Tutukov, and Yungelson (1997); Livio (2000), and references therein). Most of these systems are undetectable because of their very low intrinsic luminosity. However, thanks to an increase in luminosity due to viscous heating (Webbink and Iben 1988; Iben, Tutukov, and Fedorova 1998), perhaps a very few can be seen just before merger, due to an occultation-modulated light curve.

It is commonly understood (e.g., Tutukov and Yungelson (1979), Iben and Tutukov (1984), Benz et al. (1990), Rasio & Shapiro (1995), Mochkovitch, Guerrero & Segretain

(1997)) that if two CO WDs merge, the less massive component disrupts into an inflated disk around its companion. In this situation it has been argued that, due to a high effective accretion rate from the disk, an off-center carbon ignition occurs and the more massive star will be converted into an oxygen-neon-magnesium (ONeMg) WD (Nomoto & Iben (1985), Saio & Nomoto (1985), Kawai, Saio & Nomoto (1987), Timmes, Woosley & Taam (1994), Saio & Nomoto (1998)). These discussions do not take into account many of the complexities involved in the merger process (see, e.g., Iben (1988)). Perhaps one of the largest uncertainties plaguing the one dimensional simulations which attempt to address the problem is the unknown rate at which angular momentum diffuses out of the thick disk, allowing matter from the disk to settle onto the white dwarf and adopt a structure describable by a traditional one-dimensional model.

In this paper, we first present results of numerical experiments in which CO-rich matter is accreted radially by an initially "cooled-down" CO WD of 0.8 $M_\odot$ at rates in the range $10^{-5} - 10^{-8} M_\odot$ yr^{-1}. We explore in detail the thermal response of the accreting structure and point out the main physical parameters which drive the accretion process and determine the final outcome. These experiments provide a reference point for understanding results of further computations in which the lifting effect of rotation is taken into account. In choosing an initially cooled-down structure, we ignore the possibility that viscous heating prior to merger may be significant, but this is legitimate since there is at present no theoretical or experimental framework for estimating the magnitude of the relevant turbulent viscosity.

The plan of the work is as follows: in §2 we present the input physics and the adopted numerical techniques; in §3 we discuss the evolution of the accreting structure as a function of the accretion rate for standard (non-rotating) models; in §4 the lifting effect of rotation on the evolution of accreting models is discussed. Conclusions are summarized in §5.

2. Input Physics

The accretion experiments have been computed with an updated version of the FRANEC code (Chieffi & Straniero 1989), the main differences being discussed by Cassisi, Iben & Tornambé (1998). The equation of state is that computed by Straniero (1988) with succeeding upgrades; for the radiative low temperature opacities (T <12000 K) we adopt the tables provided by Alexander & Fergusson (1994) whereas for higher temperatures the tables provided by Huebner et al. (1977) are used. The contribution of conductive opacities has been included following the prescriptions by Mitake, Ichimaru & Itoh (1984) and Itoh, Hayashi, & Kohyama (1993). The accretion process has been computed assuming that the accreted matter has the same specific entropy as the matter at the surface of the WD (for a discussion of this topic see Taam (1980a,b), Iben (1982), Nomoto & Iben (1985)). We have adopted values of the accretion rate in the range $10^{-8} \div 10^{-5}$ $M_{\odot}$ yr^{-1}; the upper limit is an estimate of the maximum accretion rate at which the transferred matter is accepted by the accreting WD (Eddington limit), whereas the lower limit has been fixed so that the accretion process can produce a SN Ia event well before the onset of crystallization in the inner zones of the WD. The chemical composition of the accreted matter has been chosen to be equal to the chemical composition of the matter in the surface layers of the CO WD, namely $X_{^{12}C} = 0.507$, $X_{^{16}O} = 0.482$ and $X_{^{20}Ne} = 0.011$.

EDITOR: PLACE FIGURE 1 HERE.

3. Accretion with Standard Conditions

3.1. The Initial Model

The initial model is a 0.8 $M_\odot$ CO WD obtained by evolving a solar metallicity pure He star from the helium main sequence up to the cooling sequence (for more detail see Limongi & Tornambé (1991)). In the computation of the central helium-burning stage, semiconvection has been accounted for but breathing pulses at the border of the convective helium core have been neglected, as suggested by the results of Caputo et al. (1989).

When the model reaches the cooling sequence and the helium-burning shell switches off, the oxygen profile in the core exhibits a maximum and the carbon profile exhibits a minimum (see *panel a* in Fig. 1). This particular feature forms when, after the exhaustion of helium at the center, the radiative helium-burning shell goes through the region where helium was partially depleted during the outward extension of the convective helium core in the central helium-burning stage; in this zone, due to the reduction in the local helium abundance, α-captures on ^{12}C compete with 3α reactions. The extension in mass of this oxygen-enriched region depends on the efficiency of semiconvection, while the level of the peak depends on the adopted cross section for the $^{12}\mathrm{C}(\alpha,\gamma)^{16}\mathrm{O}$ reaction. Adopting the prescriptions in Salaris et al. (1997), the chemical profiles have been modified as in *panel b* of Fig. 1 and then the cooling phase has been computed. The physical characteristics of the cool model are: $\log(L/L_\odot) = -2.858$, $\log(T_{\rm eff}) = 4.049$, $\log(\rho_{\rm c}) = 7.036$, and $\log(T_{\rm c}) = 7.015$.

3.2. Time Scales of Relevance for an Accreting White Dwarf

The thermal evolution of a CO WD accreting CO-rich matter can be discussed in terms of several relevant time scales. For example, the final outcome of the accretion process can be understood by examining the behavior in time of the ratio of a thermal diffusion time scale (Henyey & L'Ecuyer 1969) and a compressional heating time scale (Sugimoto &

Nomoto 1977, Nomoto 1982a)

Ignoring all but gravothermal energy generation, conservation of energy requires that

$$\rho\left(\frac{dU}{dt}+P\frac{dV}{dt}\right)=-\nabla\cdot\mathbf{F}. \tag{1}$$

On the left hand side of this equation, U is the thermal energy per unit mass, P is the pressure, V is the specific volume ($V=1/\rho$), ρ is the density, and derivatives with respect to time are co-moving derivatives in Lagrangian coordinates. On the right hand side, assuming that energy flow is by radiation and conduction only,

$$\mathbf{F}=-\frac{16\sigma}{3}\frac{T^3}{\kappa\rho}\frac{dT}{dr}\hat{\mathbf{r}}, \tag{2}$$

where T is the temperature, σ is the Stefan-Boltzmann constant, κ is the opacity, and $\hat{\mathbf{r}}$ is a unit vector in the radial direction.

A local compressional heating time scale can be defined by setting the left hand side of eq. (1) equal to zero, giving

$$\frac{1}{\tau_{\rm comp}}=\left(\frac{1}{U}\frac{dU}{dt}\right)_{\rm adiabatic}=\left(\frac{P}{\rho U}\right)\frac{d\ \ln\rho}{dt} \tag{3}$$

Since the quantity $\left(\frac{P}{\rho U}\right)$ is nearly constant, varying in value from 1 (electrons with non-relativistic velocities) to $\frac{2}{3}$ (relativistically degenerate electrons), it is reasonable to adopt the simpler expression $\frac{1}{\tau_{\rm comp}}=\frac{d\ \ln\rho}{dt}$.

Nomoto & Sugimoto (1977) set

$$\frac{1}{\tau_{\rm comp}}=\frac{d\ \ln\rho}{dt}=\left(\frac{\partial\ \ln\rho}{\partial t}\right)_q-\left(\frac{\partial\ \ln\rho}{\partial \ln M_r}\right)_t\frac{d\ln M}{dt}, \tag{4}$$

where M is the total mass, M_r is the mass at radius r, and differentiation is with respect to mass fraction $q=\frac{M_r}{M}$ and time t as independent variables. Neglecting the first term in eq. (4), Nomoto & Sugimoto adopt

$$\frac{1}{\tau_{\rm comp}}\sim-\left(\frac{\partial\ \ln\rho}{\partial \ln M_r}\right)_t\frac{d\ \ln M}{dt}=\frac{GM_r^2}{4\pi r^4P}\left(\frac{\partial\ \ln\rho}{\partial\ \ln P}\right)_t\frac{1}{\tau_{\rm acc}}, \tag{5}$$

where

$$\tau_{\rm acc} = \left(\frac{d\ \ln M}{dt}\right)^{-1} \tag{6}$$

is the time scale for accretion.

Differentiating with respect to q and M as independent variables, Nomoto (1982a) gives

$$\frac{1}{\tau_{\rm comp}} = \left(\frac{d\ \ln\rho}{dt}\right)_{M_r} = \left[\left(\frac{\partial\ \ln\rho}{\partial \ln M}\right)_q - \left(\frac{\partial\ \ln\rho}{\partial \ln q}\right)_M\right]\frac{1}{\tau_{\rm acc}}, \tag{7}$$

showing that, in all approximations, $\tau_{\rm comp}$ is proportional to $\tau_{\rm acc}$.

A local thermal diffusion time scale can be defined as the time required by a thermal signal to propagate over a specified distance. Equations (1) and (2) give

$$\rho\left(\frac{dU}{dt} + P\frac{dV}{dt}\right) = \rho C_P\frac{dT}{dt} - \left(\frac{\partial\ \ln\rho}{\partial\ \ln P}\right)_T\frac{dP}{dt} = \left(\frac{d}{dr} + \frac{2}{r}\right)\left(\frac{16\sigma}{3}\frac{T^3}{\kappa\rho}\frac{dT}{dr}\right), \tag{8}$$

where C_P is the specific heat at constant pressure. If we set $\frac{dP}{dt} = 0$, neglect $\frac{2}{r}$ relative to $\frac{d}{dr}$, and assume that $\frac{T^3}{\kappa\rho}$ varies much less rapidly with distance than $\frac{dT}{dr}$, then

$$\frac{dT}{dt} \sim D\frac{d^2T}{dr^2}, \tag{9}$$

where

$$D = K^2 = \frac{16\sigma}{3}\frac{T^3}{\kappa C_P\rho^2}. \tag{10}$$

Equation (9) is the well known equation for the diffusion of heat and its solution for many situations is proportional to (e.g., Margenau & Murphy 1943)

$$\exp\left(-\frac{\delta r^2}{4Dt}\right), \tag{11}$$

where δr is the distance from an initial delta-function perturbation in T. This motivates the choice of

$$\tau_{{\rm diff},\delta r} = \frac{\delta r^2}{4D} \tag{12}$$

as a measure of, or "time scale" for, the diffusion of heat across the distance δr.

As suggested by Sugimoto (1970), an appropriate length scale is the local pressure scale height H_P, leading to a "local" diffusion time scale

$$\tau_{\rm diff,loc} = \frac{H_P^2}{4D}, \tag{13}$$

(Sugimoto chooses a value 4 times larger than this). One might naively assume that a time scale for the propagation of heat over many scale heights is given by the sum of local time scales over these scale heights. However, as discussed by Henyey & L'Ecuyer (1969), the appropriate approximation is instead

$$\tau_{\rm diff,glob} = \left(\int_{r_1}^{r_2} \frac{1}{2K} dr\right)^2 = \frac{3}{64\sigma}\left[\int_{r_1}^{r_2} \left(\frac{\kappa C_p}{T^3}\right)^{1/2} \rho dr\right]^2, \tag{14}$$

where the integral extends from r_1 to r_2.

In the following, we will make use of a "global" compressional heating timescale defined as $\tau_{\rm ch} = \tau_{\rm acc}$ and of a "global" diffusion time scale $\tau_{\rm diff}$ equal to the value of $\tau_{\rm diff,glob}$ given by eq. (14) when $r_1 = 0$ and $r_2 = R$, where R is the radius of the star.

The gravitational energy released by accreted matter is partly stored in layers near the surface as thermal energy, but partly diffuses inward, increasing the thermal content of layers ever deeper below the surface. If $\tau_{\rm diff} > \tau_{\rm ch}$, heating of layers near the surface may lead to the off-center ignition of carbon, well before the white dwarf reaches the Chandrasekhar limit (Nomoto 1982a,b, Nomoto & Iben 1985). If $\tau_{\rm diff} < \tau_{\rm ch}$, energy can be transferred inward efficiently enough that carbon ignition occurs at the center or, if oxygen has replaced carbon at the center, at the base of a carbon-rich layer (Isern et al. 1983, Hernanz et al. 1988).

Choosing $D = R_{\rm star} \sim 10^{-2} R_\odot$, $T = T_{\rm c} \sim 10^7$ K (isothermal structure), $C_p \sim 10^7$ erg/g K, ρ equal to the average density of the structure ($\sim 10^6$ g/cm^3), and κ equal to the mean

conductive opacity ($\kappa \sim 10^{-4}$ cm^2/g), our initial model is characterized by $\tau_{\rm diff} \sim 3 \times 10^7$ yr. Insisting that $\tau_{\rm diff} = \tau_{\rm ch}$, the maximum value for the accretion rate suitable for the efficient transfer toward the inner zones of gravitational energy released by accretion can be estimated as $\dot{M}_{\rm max} \sim 3 \times 10^{-8} M_\odot$ yr^{-1}. It follows that, if $\dot{M} < \dot{M}_{\rm max}$, the thermal energy excess in the outer layers is transferred to the interior and carbon burning is ignited at the center.

The value of $\tau_{\rm diff}$ just estimated refers to the initial model. Since $\tau_{\rm diff}$ actually evolves in time as a consequence of the evolution of the physical conditions in the accreting structure, it is necessary to examine its value in the evolving models.

EDITOR: PLACE FIGURE 2 HERE.

In Fig. 2, the evolution of $\tau_{\rm diff}$ (solid lines) is shown in comparison with the evolution of $\tau_{\rm ch}$ (dashed lines) for all of the models computed in the present work, as listed in Table 1. It is evident that, for $\dot{M} < \dot{M}_{\rm max}$ (*panel i*), the mass of the accreting WD reaches the Chandrasekhar limit, so that central carbon burning occurs. It is apparent also that, for the cases with $\dot{M}_{\rm max} < \dot{M} < 10^{-6}$ $M_\odot$ yr^{-1} (*panels e* to *h*) , the gravitational energy deposited in outer layers is transferred efficiently toward the center since, during the accretion process, the compressional heating time scale increases while the thermal diffusion time scale decreases until the ratio of the two time scales is reversed. This occurrence can be easily explained by observing that, on increasing the total mass, the radius and the conductive opacity of the accreting structure decrease while density and temperature increase. This behavior is common to the entire set of computed models, but if $\dot{M} > 10^{-6}$ $M_\odot$ yr^{-1} , carbon-burning ignition occurs in the outer layers well before a significant amount of the deposited gravitational energy can be transferred toward the center. Fig. 2 discloses further that, for small enough accretion rates (say, less than $5 \times 10^{-7} M_\odot$ yr^{-1}), the thermal

diffusion time scale profile has two different slopes, the inflection point corresponding to the time when the thermal wave reaches the center.

EDITOR: PLACE FIGURE 3 HERE.

This behavior can be better appreciated in Fig. 3 where the evolution of the mass coordinates of the maximum temperature ($M_{T-\max}$) and of the central temperature ($T_{\rm c}$) are reported together with $\tau_{\rm diff}$ as functions of the total mass of the accreting structure for the case $\dot{M} = 5 \times 10^{-8}\ M_\odot\ {\rm yr}^{-1}$. Where the central temperature increases most rapidly with mass (mass coordinate $\sim 1.05 \pm 0.05\ M_\odot$), the rate of change in the slope of $\tau_{\rm diff}$ decreases rapidly, becoming almost flat. The maximum in temperature does not reach the center until the whole structure has become isothermal. Thereafter, the evolution of the central temperature is driven by homologous compression.

The final sudden increase of the central temperature and the corresponding decrease in $\tau_{\rm diff}$ when the total mass of the accreting WD reaches $\sim 1.35\ M_\odot$ is a consequence of the strong compression due to the approach to the Chandrasekhar mass.

A discussion of global behavior can also be conducted in terms of local time scales. By way of illustration, we examine the cases of accretion at rates marking the boundaries of the region we have explored, namely, $10^{-5}\ M_\odot\ {\rm yr}^{-1}$ and $10^{-8}\ M_\odot\ {\rm yr}^{-1}$. In Fig. 4, the evolution of the temperature, the local compressional heating time scale $\tau_{\rm ch,loc}$ given by eq. (2), and of two ratios involving $\tau_{\rm ch,loc}$, $\tau_{\rm diff,loc}$ given by eq. (11), and $\tau_{\rm evo}$, the time elapsed since the beginning of the experiment, are shown for the case $10^{-5}\ M_\odot\ {\rm yr}^{-1}$.

EDITOR: PLACE FIGURE 4 HERE.

In the inner regions ($M < 0.65\ M_\odot$), the heat diffusion time scale is long compared with the compressional heating time scale, so the increase in temperature is due entirely to

local compressional heating. In central regions ($0.65 < M < 0.8\ M_\odot$), the heat diffusion time scale decreases in the outward direction to become comparable to the compressional heating time scale, and heating is due to a combination of compressional heating and inward diffusion, the contribution of diffusion increasing outward with respect to the contribution of compression. In the outermost accreted layers ($M > 0.8\ M_\odot$), $\tau_{\rm diff,loc}$ is everywhere smaller than $\tau_{\rm ch,loc}$ and, since also everywhere $\tau_{\rm diff,loc} < \tau_{\rm evo}$, diffusion efficiently redistributes energy liberated by compression both inward and outward. The peaks in the temperature profiles show that the "watershed" marking the place where the heat flow changes directions is approximately at the center of the accreted layer.

Figure 5 shows the evolution of the same quantities displayed in Fig. 4, but for the case $10^{-8}\ M_\odot\ {\rm yr}^{-1}$. In this case, $\tau_{\rm diff,loc}$ is always larger than $\tau_{\rm ch,loc}$ everywhere in the interior; as $\tau_{\rm evo}$ increases, compressional energy released everywhere is redistributed in such a way that the whole structure becomes nearly isothermal.

It is worth pointing out that, over the matter in the initial white dwarf, the mass averaged value of $\tau_{\rm ch}$ is essentially $\tau_{\rm acc}$, whereas, in the accreted layer, $\tau_{\rm ch}$ is everywhere much less than $\tau_{\rm acc}$. So, what we really do when we compare $\tau_{\rm diff,glob}$ with $\tau_{\rm acc}$ is compare the time it takes energy deposited in accreted layers to make its way into the deep interior of the original white dwarf with the time it would take these layers to heat up without inward diffusion.

EDITOR: PLACE FIGURE 6 HERE.

3.3. The Accretion Experiments

In Fig. 6 we plot the evolution of the accreting structures in the HR diagram while in Fig. 7 we report the evolution of the surface radius as a function of the total mass for all the models listed in Table 1. It is evident that, at the beginning of the accretion process, the structure returns along the cooling sequence discussed in §3.1 and expands since the gravitational energy deposited at the surface causes a local increase in temperature and, hence, in luminosity. It is important to keep in mind that the initial WD is a very compressed isothermal structure so that the local efficiency of the inward thermal diffusion is very small ($\tau_{\rm diff}$ is very large); indeed, all of the energy delivered by the accreted matter is locally stored as thermal energy. The increase in pressure related to the increase in temperature leads to a rapid expansion of the outer layers; the expansion induces a decrease in the local density while the continuous deposition of matter produces an increase in the local temperature. In fact, the value of $\tau_{\rm diff}$ in surface layers begins to decrease and, when the energy excess can be transferred to the underlying zones, that is, when the local $\tau_{\rm diff}$ becomes less than $\tau_{\rm ch}$, the structure begins to contract. As is clearly shown in Figs. 6 and 7, the larger the accretion rate, the larger is the radius at the end of the expansion phase and the larger are the luminosity and the effective temperature; as the accretion rate is increased, the rate at which gravitational energy is deposited in surface layers is increased and, hence, the induced expansion becomes larger.

EDITOR: PLACE FIGURE **??** HERE.

EDITOR: PLACE FIGURE 7 HERE.

In Fig. 8, we plot the evolution of the center of the accreting WD in the $\rho - T$ plane and in Table 1 we report for each adopted value of the accretion rate the final mass (in

$M_\odot$), the mass coordinate (in $M_\odot$) at which carbon burning is ignited, and the value of temperature (in K) and density (in g cm^{-3}) at this point. Only for $\dot{M}$ smaller than 10^{-6} $M_\odot$ yr^{-1} does central carbon ignition occur. Three different phases can be distinguished in the thermal evolution of models which ignite carbon burning at the center:

EDITOR: PLACE FIGURE 8 HERE.

- the first phase, during which the thermal evolution of the center is determined by homologous compression. In this phase, the increase in mass of the WD induces the compression of the whole structure while the gravitational energy delivered by the accreted matter is stored in the outermost layers;
- the second phase, characterized by a rapid increase in the central temperature. This rapid increase in central temperature is a consequence of the fact that the gravitational energy initially localized in outer layers has diffused to the center. During this phase, homologous compression continues to be active and drives the evolution of the central density. This phase is concluded when the structure becomes almost isothermal;
- the third phase, during which thermal diffusion and homologous compression are both effective. At this stage, the structure is isothermal, as it was when the accretion process began, but now the temperature level is higher; as a consequence, gravitational energy is not stored for long in outer layers but is almost immediately transferred to underlying zones (see the drop in $\tau_{\rm diff}$ in Fig. 3 from the first to the third phases). In addition, the gravitational energy delivered by the accreted matter is negligible with respect to the heating produced by homologous compression, the efficiency of which is independent of the thermal content of the accreting structure; as a consequence, during this phase, homologous compression becomes the leading factor which governs the increase in the interior temperature.

It is interesting that the rate of increase in the central temperature in the third phase is smaller than that in the first one, whereas one might reasonably expect that the combined effect of both thermal diffusion and homologous compression would produce a more rapid increase in the central temperature during the third phase. The actual behavior may be explained by observing that the rate of energy loss via plasma neutrino emission increases with increasing temperature, thus leading to a reduced efficiency of heating of the central regions where temperatures are highest.

In Fig. 9 are plotted, for every adopted accretion rate, temperature profiles at different times during the accretion process. For models with accretion rates larger than 10^{-6} $M_{\odot}$ yr^{-1}, the evolution of both temperature and density at the center is determined only by homologous compression. In fact, for such models, the thermal excess introduced by the accretion process into outer layers does not reach the center before runaway carbon burning (initiated at the point where the temperature is at a maximum) terminates the process. The model accreting matter at $\dot{M} = 2 \times 10^{-6}$ $M_{\odot}$ yr^{-1} defines a transition line: the physical conditions suitable for carbon burning are achieved first near the center (see panel d) in Fig. 9, M = 0.2 $M_{\odot}$), but quite soon also in outer layers where the maximum in temperature is located ($M = 1.375$ $M_{\odot}$). As time goes on, however, the rate of delivery of nuclear energy increases more quickly in the outer layers than in the deep interior and the thermonuclear runaway occurs first in the outer layers.

EDITOR: PLACE FIGURE 9 HERE.

In Fig. 10 are plotted the density profiles for the same models described in Fig. 9. The initial expansion phase is clearly shown by the decrease in the surface density whereas the action of the homologous compression is evidenced by the self-similar evolution of the density profiles. The same behavior is evident in the evolution of the temperature profiles

for the case $\dot{M} = 10^{-5}\ M_{\odot}\ \mathrm{yr}^{-1}$; as time increases, the temperature level of the inner regions increases homologously while the continuous accretion process induces the formation of a peak in temperature in the outer layers.

EDITOR: PLACE FIGURE 10 HERE.

Models with $10^{-7} < \dot{\mathrm{M}} \leq 10^{-6} M_{\odot}\ \mathrm{yr}^{-1}$ (*panels e* and *f* in Fig. 9) achieve the conditions for carbon ignition in the inner zone when the maximum in temperature is still located in outer layers. This is also apparent from an inspection of Fig. 11, where we report profiles in the $\rho - T$ plane for the models which have achieved ignition conditions. This behavior is due to the fact that the energy loss rate via plasma neutrinos, $\varepsilon_{\mathrm{plasma}-\nu} \propto T^3$, is very large near the mass coordinate where the maximum in temperature is located. Hence, the gravitational energy delivered by the accreted matter causes a steepening of the temperature gradient and, paradoxically, the energy-loss sink due to $\varepsilon_{\mathrm{plasma}-\nu}$ becomes deeper, reducing the amount of heat which can be transferred toward the center. Due to the effect of plasma neutrino losses, there is no carbon ignition for densities in the range $10^7 - 10^9$ g/cm^3.

EDITOR: PLACE FIGURE 11 HERE.

Models with accretion rates smaller than $\dot{\mathrm{M}} \leq 10^{-7}\ M_{\odot}\ \mathrm{yr}^{-1}$ succeed in removing the energy excess deposited in outer layers because the gravitational energy is deposited more slowly than it diffuses inward. The surface energy reservoir is smaller and, hence, the energy losses via plasma neutrinos are smaller, so that the heat transfer inward is very efficient. In addition, the homologous compression induced by the accretion process is less rapid and the accreting star approaches the Chandrasekhar mass without carbon burning being ignited at a significant level anywhere within the structure. On the other hand, as the total mass approaches M_{Ch} , the rate of contraction becomes larger and the effect of

the induced compression, which is larger at the center, determines the physical conditions suitable for a central carbon ignition. During subsequent evolution under highly degenerate physical conditions, the energy delivered by carbon burning is stored locally, increasing the local temperature; the onset of convection (see *panels f* to *i* in Fig. 9) marks the onset of the thermonuclear runaway which will cause the disruption of the accreting star as a Type Ia Supernova. Although in these models the leading parameter in the evolution up to the carbon-ignition stage is the compression induced by strong contraction, the matter deposited on the surface plays a not completely negligible role in determining the ignition conditions. On decreasing the accretion rate, the density at which carbon ignition occurs becomes larger and, correspondingly, the temperature becomes smaller.

4. The Effect of Rotation

4.1. Physical Assumptions and Numerical Procedures

To explore the effect of stellar rotation on the thermal response of CO WDs accreting matter we have included the lifting effect into the hydrostatic equilibrium equation according to the prescriptions in Dominguez et al. (1996):

$$\frac{dP}{dr} = -\frac{GM}{R^2}\rho\,(1-f)\,, \tag{15}$$

where f is the ratio between the centrifugal and gravitational forces $f = \frac{F_c}{F_g} = \frac{\omega^2 r}{g}$. In order to maintain the spherical symmetry in the treatment of the problem, the centrifugal force on a generic mass element dm is averaged over a sphere of radius r so that its value is provided by the following relation:

$$< F_c >= \frac{\int_{S_r} F_c dS_r}{S_r} = dm\frac{\int_0^\pi 2\pi\omega^2 r^3 \sin^2\theta d\theta}{4\pi r^2} = \frac{\pi}{4} dm\omega^2 r. \tag{16}$$

This treatment is equivalent to those by Kippenhahn & Thomas (1970) and Endal &

Sofia (1976, 1978) except that we neglect the corrective factor included by these authors in the expression for the radiative gradient (see Dominguez et al. 1996). Since WDs are chemically fairly homogeneous and are very compact objects, the efficiency of angular momentum redistribution may be large enough (Maeder & Meynet 2000) that the accreting WD can be treated as a rigid rotator, and we assume this to be the case.

As discussed by Tassoul (1978), a rotating fluid undergoes instabilities which must be accounted for in a realistic description of the phenomenon. By adopting a rigid-rotator model, neither the Solberg nor the Goldreich-Schubert-Fricke instabilities arise. On the other hand, rotation could induce deformations of the equipotential surfaces in a such a way that meridional circulations on a large scale arise (von Zeipel paradox). In this case, deviations from spherical symmetry can be checked by computing a dimensionless quantity γ defined as the ratio between rotational and gravitational energy ($\gamma = E_{\rm rot}/E_{\rm g}$). If $\gamma > 0.14$, the equilibrium configuration is no longer spherical and meridional circulations cannot be neglected. In our computations, the γ parameter is always smaller than 0.1, so meridional circulations have not been taken into account. Finally, if the centrifugal force acting on a mass element dm becomes larger than the gravitational force ($f > 1$ in eq. 3), this element will experience a radial acceleration outward, achieving a velocity greater than the escape velocity (Roche instability) and the accretion process will be terminated. The angular velocity for which $f = 1$ is defined as the *critical angular velocity* $\omega_{\rm crit}$, and its value is given by

$$\omega_{\rm crit} = \sqrt{g/r}, \tag{17}$$

where r is the distance from the center to the mass element dm and g is the local value of the gravitational acceleration. This instability has been checked in detail during the evolution of the accreting models and will be addressed in the discussion of results.

In the present computation, it is assumed that the accreted matter flows to the WD

from a co-rotating accretion disk and that the deposited material has the specific angular momentum $j_{\rm D} = \omega d^2$, where d is the radius of the accreting WD and ω is the instantaneous angular velocity of the WD. The rate of change of the angular velocity ω of the WD model is then given by $\dfrac{d\omega}{dt} = \dfrac{j}{I}\dot{M}$, where I is the moment of inertia of the model.

The initial angular velocity, and, as a consequence, the initial total angular momentum of the accreting WD have been fixed parametrically by assuming that $\omega = \alpha\ \omega_{\rm crit,0}$, where $\omega_{\rm crit,0}$ is the initial value of $\omega_{\rm crit}$ and α is a constant (< 1). In our case, $\omega_{\rm crit,0} = 0.625$ rad/s and, in the computations, we have adopted $\alpha = 0.1$, 0.3, 0.5, 0.7, and 0.9.

4.2. Numerical Results

The inclusion of rotation in the hydrostatic equilibrium equation has a "lifting" effect, reducing the local value of pressure throughout the structure in such a way that the accreting star is both less dense and cooler than in the standard case (rotation neglected). While the density is only moderately decreased, the decrease in temperature throughout the accreting structure leads to a large enough increase in the thermal diffusion time scale to have a noticeable effect on the evolutionary behavior of the model. This is clearly shown in Fig. 12 where the initial value of $\tau_{\rm diff}$ is plotted as a function of the initial angular velocity.

EDITOR: PLACE FIGURE 13 HERE.

On the other hand, the effect of compression induced by the accretion process is only slightly modified by the inclusion of rotation. Since $\tau_{\rm diff}$ is far more sensitive to the inclusion of rotation than is $\tau_{\rm ch}$, an increase in the initial angular velocity of the WD always means a decrease in the value of the accretion rate below which central carbon ignition (as defined in §3.2) will occur. Evolution during the expansion phase at the beginning of the accretion

process is modified in a similar way. Since the initial expansion process is totally driven by the ratio $\tau_{\rm diff}/\tau_{\rm ch}$, for a fixed accretion rate (that is, for a given amount of gravitational energy delivered onto the WD per unit of time), the local energy excess in surface layers and, hence, the induced expansion become larger, the larger the initial angular velocity. This dependence is illustrated in Fig. 13, where the evolution of surface radius versus total mass is shown as a function of initial angular velocity.

EDITOR: PLACE FIGURE **??** HERE.

When rotation is not taken into account, the expansion comes to a halt due to a decrease in $\tau_{\rm diff}$ in surface layers; gravitational energy is transferred efficiently to underlying zones from surface layers, which consequently begin to contract (see the discussion in §3). When rotation is taken into account, the Roche instability can occur, leading to an expansion phase during which $\omega_{\rm crit}$ decreases in layers near the surface. In this case, the accreting structure may become gravitationally unbound after only a small amount of matter has been accreted. In Fig. 14 are shown the time evolution of several quantities for the model with $\dot{M} = 10^{-8} M_{\odot}$ yr^{-1} and ω_0 =0.5 $\omega_{\rm crit,0}$. The quantities are the thermal diffusion time scale near the surface (panel a), the surface temperature (panel b), the radius (panel c). Panel d shows the evolution of the WD angular velocity ω (lower curve) and of the critical angular velocity in the outermost layers $\omega_{\rm crit,s}$. As the surface radius increases, $\omega_{\rm crit,s}$ decreases while, because of the deposition of angular momentum by accreted matter, ω increases almost linearly with increasing WD mass.

EDITOR: PLACE FIGURE 14 HERE.

From these results, it follows that, for each value of $\dot{M}$, there exists a threshold value $\omega_{\rm th}$ for ω_0 such that, if $\omega_0 > \omega_{th}$, the accreting structure becomes gravitationally unbound

due to the expansion during the first phase of the accretion process. In the $\dot{M} - \omega_0$ plane of Fig. 15, the shaded region gives the initial angular velocity and accretion rates for which the accreting WD becomes gravitationally unbound when its total mass approaches 1.4 $M_\odot$.

EDITOR: PLACE FIGURE 15 HERE.

Models which survive the expansion during the first phase of the accretion process recontract since the decrease in $\tau_{\rm diff}$ in outer layers leads to an efficient transfer inward of the gravitational energy released. During this phase, the evolution of the accreting structure resembles the evolution of a non-rotating model, although, for a given value of the accretion rate, the whole structure is cooler and less dense for larger ω_0 . In Fig. 16, we show the same quantities as in Fig. 14 for a case in which the accretion rate is the same ($\dot{M} = 10^{-8} M_\odot$ yr^{-1}), but in which the initial angular velocity is smaller ($\omega_0/\omega_{\rm crit,0} = 0.1$). In this case, the initial expansion is not large enough to significantly slow the decrease in $\tau_{\rm diff}$, and both ω and $\omega_{\rm crit,s}$ increase steadily with increasing WD mass as the energy excess deposited in outer layers is efficiently transferred toward the center, as is clearly depicted in Fig. 17 where temperature profiles for various models during the accretion process are shown.

EDITOR: PLACE FIGURE 16 HERE.

As detailed in Fig. 16, the accreting WD spins up as its radius increases, with both ω and $\omega_{\rm crit,s}$ increasing steadily; as a result, the temperature level throughout the WD increases homologously (see also Fig. 17). When the WD mass reaches ~ 1.3 $M_\odot$, the centrifugal force begins to compete with the gravitational force; thereafter, the increase in the total angular momentum of the structure causes the surface layers of the WD to expand and the compression induced by the accreted matter is no longer able to balance

the radiative losses. As a consequence, the entire structure cools down (see the last profile in Fig. 17)! Notice further that the expansion produces a decrease in $\omega_{\rm crit}$ to the extent that the accreting structure becomes gravitationally unbound; the accretion process comes to a halt.

EDITOR: PLACE FIGURE 17 HERE.

It thus appears that the occurrence of the Roche instability prevents the accreting models from achieving the physical conditions necessary for the ignition of carbon; the accreting structures are not only too cool but, in addition, the centrifugal force due to rotation prevents the contraction in interior regions which produce heating by the conversion of gravitational potential energy.

4.3. The Dependence of the Final Outcome on $j_{\rm D}$

The scenario summarized in Fig. 15 depends on the amount of angular momentum deposited by the accreted matter: in fact, the increase in the angular velocity, particularly during the early phase of the accretion process, is totally controlled by the deposition of angular momentum. In order to make this point clearer, we have re-computed the previously discussed models assuming that the accreted matter flows to the WD from an accretion disk at rest ($j_{\rm D} = 0$). In Fig. 18, we report the evolution of the surface radius for models accreting CO-rich matter at the rate $\dot{M} = 10^{-7}\ M_{\odot}\ {\rm yr}^{-1}$ with different initial angular velocities, assuming that the accreted matter deposits (dashed lines) or does not deposit (solid lines) angular momentum. It is clear that, if angular momentum is not added, the accreting structure with initial angular velocity smaller than 0.9 $\omega_{\rm crit,0}$ survives the initial expansion and thereafter contracts as a consequence of the increase in the total mass. In addition, if $j_{\rm D} = 0$, for ω_0 in the range $0.3 \div 0.9\ \omega_{\rm crit,0}$, the accreting structure ignites

carbon burning at the center since the total mass is larger than 1.4 $M_\odot$. It is also clear that, the larger the initial value of the angular velocity, the larger is the final total mass of the accreting WD. This occurrence is consistent with the known fact that the Chandrasekhar mass for rotating structure is larger than that for non rotating models, depending strongly on the angular velocity (see Anand 1968, Ostriker and Bodenheimer 1968).

EDITOR: PLACE FIGURE 18 HERE.

By assuming that the accreted matter does not deposit angular momentum, the morphology of the $\dot{M}$ -ω_0 plane changes from that shown in Fig. 15 to that shown in Fig. 19. The changes are worth emphasizing:

- for large values of both ω_0 and $\dot{M}$ (the region labeled "$M_f < 1\ M_\odot$"), the accreting models experience the Roche instability when only a small amount of matter has been accreted ($\Delta M_{\rm acc} \leq 0.1\ M_\odot$). This zone corresponds to the non-shaded region in Fig. 15, so that its lower boundary represents the $\omega_{\rm th}$ previously defined;

- for large values of ω_0 and small values of $\dot{M}$ (the region labeled "$\varepsilon_{\rm n} < \varepsilon_\nu$"), the accreting structures never achieve the physical conditions necessary for carbon ignition, although they do not become gravitationally unbound. The computation of these models has been halted because the adopted input physics, in particular the equation of state, is inadequate. In any case, the final mass of the accreting structure is larger than 1.4 $M_\odot$;

- for small values of both ω_0 and $\dot{M}$ (the region labeled "Central Ignition"), the accreting structures ignite carbon burning at the center when the total mass approaches (and in some case exceeds) the non-rotating Chandrasekhar mass;

- the zone labeled "Central and Off-Center C-ignition" represents structures which ignite carbon burning both at the center and in the outer layers. This zone marks the transition between models which become gravitationally unbound and models which succeed in igniting carbon burning;

- models in the region above the dashed line and below the present $\omega_{\rm th}$ line become gravitationally unbound when the total mass of the accreting structure approaches the non-rotating Chandrasekhar mass. This region corresponds to the shaded zone in Fig. 15.

EDITOR: PLACE FIGURE 19 HERE.

It is evident that, on including the lifting effect of rotation on the evolution of a CO white dwarf accreting CO-rich matter, the zone in the $M_{\rm WD}$ - $\dot{M}$ plane suitable for a central carbon ignition becomes narrower. If matter is accreted at rest, carbon burning is ignited at the center for the same values of the accretion rate as in the standard case ($\dot{M} < 10^{-6} M_{\odot}$ yr^{-1}), but only for small values of the initial angular velocity (see Fig. 19), whereas, if the matter is accreted from a co-rotating disk, the WD never ignites carbon burning. In this latter case, the increase of the angular velocity due to the deposition of angular momentum by the accreted matter induces the expansion of the accreting structure which becomes gravitationally unbound.

4.4. The Braking Phase

Interestingly enough, rotating models with small values of both the initial ω (namely $\omega_0 < 0.3\ \omega_{\rm crit,0}$) and accretion rate (namely $\dot{M} < 10^{-7}\ M_{\odot}$ yr^{-1}) undergo the Roche instability when their total mass is of the order of the non-rotating Chandrasekhar mass.

In this case, the ratio of rotational and gravitational energies ($\gamma = E_{\rm rot}/E_{\rm g}$) approaches the critical value ~ 0.14 and, as a consequence, the accreting structure has to deform into an ellipsoidal shape (see §4.1); due to the induced deformation, the mass distribution of the white dwarf becomes anisotropic in such a way that gravitational wave radiation is emitted (see Shapiro & Teukolski 1983, 1990). The emitted waves carry away rotational energy and angular momentum and the total angular momentum of the braking structure evolves according to an exponential law $J = J_0 e^{-t/\tau}$, where J_0 is the value of the angular momentum at the beginning of the slowing down phase and τ is the time scale on which the process occurs; the latter quantity is determined by the efficiency of braking and, therefore, by the angular velocity of the structure when γ approaches the critical value. Since the intensity of the emitted GWR depends on ω^2, we assume that the braking process becomes the driving mechanism for the evolution of the accreting white dwarf when the angular velocity is of the order of 1 rad s^{-1}.

It is worth noticing that, on decreasing the total angular momentum, the effective gravity acting on a given mass element increases and, as a consequence, the whole structure experiences a contraction which produces the heating-up of the entire star. In addition, the contraction induced by the braking produces an increase in the angular velocity of the white dwarf so that the γ parameter actually remains of the order of the critical value. This means that the white dwarf continues to emit GWR copiously as it contracts.

These considerations suggest that the braking process acts as a compression mechanism and that the τ parameter in the exponential braking law can be interpreted as a compressional heating time scale; we can therefore argue that the final outcome of the braking phase depends on the ratio between τ and $\tau_{\rm diff}$, the thermal diffusion time scale of the considered structure.

In order to explore this conjecture, we have constructed an evolutionary sequence

which begins with a model at the end of the previously explored sequence with initial angular velocity $\omega_0 = 0.1\omega_{\rm crit,0} = 0.067$ rad/s and accretion rate $\dot{M} = 10^{-8}\ M_\odot\ {\rm yr}^{-1}$. In this last model, γ is of the order of the critical value, the total mass of the white dwarf is $\sim 1.42\ M_\odot$, the angular velocity is ~ 1.1 rad/s, and the value of $\tau_{\rm diff}$ is $\sim 2 \times 10^7$ yr; at this time the structure is isothermal, as shown in Fig. 17.

In order to explore the effect of GWR braking on further evolution, we choose two values of τ: $\tau = 10^7$ yr, which corresponds to a low braking efficiency, and $\tau = 10^3$ yr, which corresponds to a high braking efficiency. As discussed in Shapiro & Teukolski (1983) and in Ma (2002), the GWR-driven braking process is not important on time scales greater than 10^7 yr since, then, the slowing down is dominated by viscosity.

In the first case ($\tau = 10^7$ yr), the homologous compression induced by GWR braking produces an increase in temperature everywhere in the structure, as shown in Fig. 20, where temperature profiles for selected models are presented. When the physical conditions suitable for carbon burning ignition are achieved at the center, the released nuclear energy is stored locally, due to the high electron degeneracy; a convective core forms and grows rapidly until convection reaches the surface. The thermonuclear runaway will ultimately proceed on a dynamical time scale, causing the disruption of the white dwarf as a type I supernova.

EDITOR: PLACE FIGURE 20 HERE.

In the second case ($\tau = 10^3$ yr), the GWR-induced compression also produces a homologous increase in the temperature level throughout the structure. But, superimposed on this increase is an additional increase in layers near the surface, where a local temperature maximum forms (see Fig. 21). This secondary maximum occurs in part because matter near the surface, being less electron degenerate, has a larger specific heat. Additionally, however,

the evolution of the model occurs on a time scale smaller than the thermal diffusion time scale in surface layers, so the thermal energy released into layers near the surface remains localized in these layers. In any case, the evolution of the model is totally dominated by the homologous compression due to GWR-induced braking, and, just as in the first case, the thermonuclear runaway which has begun at the center will evolve into an explosion of supernova proportions.

EDITOR: PLACE FIGURE 21 HERE.

Thus, the final outcome in both cases is a SN Ia event, independent of the assumed GWR-braking efficiency. The only effect of a variation in the braking efficiency over a substantial range is a modest variation in the physical characteristics of matter when carbon burning first develops into a thermonuclear runaway at the center. This is made clear in Fig. 22, where we show the evolution of central characteristics in the $\rho - T$ plane for the two discussed models.

EDITOR: PLACE FIGURE 22 HERE.

5. Final Remarks

In this work, we have explored the lifting effect of rotation on the evolution of a CO WD accreting CO-rich matter from the thick disk that is initially formed during the merger of two close binary CO WDs. We find that rotation induces a cooling of the accreting structure to the extent that the final outcome of the accretion process can be significantly modified relative to the case when rotation is neglected. For a fixed value of $\dot{M}$ and an initial angular velocity of the WD larger than a critical value, the accreted matter produces

a large enough thermal energy excess in outer layers that the star itself expands to a larger radius. The induced expansion leads to a reduction of the surface gravity to the extent that the accreting structure becomes gravitationally unbound (Roche instability) and no more matter can be added. We have shown that this occurrence depends on both the accretion rate and the initial angular velocity. For large values of both $\dot{M}$ and ω_0 , the accreting WD becomes gravitationally unbound when only a small amount of mass has been added ($\Delta M_{\rm acc} \leq 0.1\ M_\odot$), whereas, for small values of both $\dot{M}$ and ω_0 , the WD attains a total mass close to 1.4 $M_\odot$ before the Roche instability sets in. We have also shown that behavior of this sort depends critically on the angular momentum carried by the accreted matter. For a fixed accretion rate, the larger the specific angular momentum of the accreted matter, the earlier does the Roche instability occur (the WD spins up more rapidly).

The behavior we describe is a consequence of the fact that the thermal diffusion time scale is very sensitive to changes in the assumed rotation rate (increasing with increasing rotation rate) whereas the compressional heating time scale is almost independent of such changes; the rate of transfer toward inner regions of the energy excess produced in outer regions by accreted matter becomes smaller and smaller with respect to the standard case (without rotation) as the rotation rate is increased. As a consequence, for a given accretion rate and WD mass, the density and temperature at the center are smaller, the larger the initial angular velocity. In addition, we find that, if the specific angular momentum of the accreted matter is equal to that in the outer layers of the WD, all the computed models become gravitationally unbound well before the physical conditions suitable for carbon burning ignition are attained anywhere in the WD structure.

For small values of both initial angular velocity and accretion rate (namely, $\omega_0 < 0.3\omega_{\rm crit,0} =\sim 0.18$ rad/s and $\dot{M} \leq 10^{-7} M_\odot$ yr^{-1}), the accreting model becomes a very fast rotator ($\omega_{\rm f} \sim 1$ rad/s) when the total mass is of the order of 1.4 $M_\odot$ and γ ($= E_{\rm rot}/E_{\rm g}$)

becomes of the order of the critical value ($\gamma_{\rm cr} \sim 0.1$). Then, the accreting WD adopts an elliptical shape and begins to emit gravitational waves which carry away both angular momentum and rotational energy. The important point is that the braking induced by GWR produces a contraction of the whole structure and, as a consequence, the WD spins up in such a way that the γ parameter continues to be of the order of the critical value.

In this way, the evolution of the structure is totally driven by the homologous compression induced by the GWR-braking process. According to our results, independently of the efficiency of braking, which means independently of the time scale on which braking occurs, the physical conditions suitable for an explosive carbon-burning ignition are attained at the center of the WD, so that a SN Ia event occurs.

For models with large ω_0 and $\dot{M}$, the Roche instability occurs when the total mass of the WD is smaller than 1.4 $M_\odot$, the exact value depending on the initial values of both the accretion rate and the angular velocity. But this result has been obtained by assuming that the accretion rate is strictly constant; in the real world, the WD will continue to accrete, but at a smaller rate. As the Roche instability is approached, the accretion rate drops, the angular momentum of the WD increases less rapidly, and the rate of producing an energy excess in the surface layers decreases. Thus, a self-regulatory mechanism prevents the gravitational instability from actually taking place. Rotation acts as a tuning mechanism for the accretion rate in such a way that the accreting structure can continue to accept mass even in the case of a very large initial accretion rate. We address the details of this topic in a forthcoming paper. For now, it is sufficing to observe that, although the accretion rate decreases due to the lifting effect of rotation, the total angular momentum and, as a consequence, the angular velocity of the WD must increase; the WD will become a fast rotator. Gravitational wave radiation becomes competitive with thermal diffusion when the angular velocity of the WD attains a value of the order of 1 rad s^{-1}, and, thereafter,

GWR-induced braking leads to the physical conditions suitable for carbon-burning ignition in the center and, hence, to a SN Ia event.

6. Acknowledgements

We thank the referee for pointing to appropriate work in the literature and for persuading us to examine various time scales more closely.

REFERENCES

Anand, S. P. S. 1968, ApJ, 153, 135

Arnett, W. D. 1969, Ap.Space.Sci., 5, 150

Alexander, D. R. & Ferguson, J. W. 1994, ApJ, 437, 879

Benz, W., Cameron, A. G. W., Press, W. H. & Bowers, R. L., 1990 Ap.J, 348, 647

Caputo, F., Castellani, V., Chieffi, A., Pulone, L. & Tornambé, A. 1989, ApJ, 340, 241

Cassisi, S., Iben, I., Jr. & Tornambè, A. 1998, ApJ, 496, 376

Chieffi, A. & Straniero, O. 1989, ApJS, 71, 47

Dominguez, I., Straniero, O., Tornambé, A. & Isern, J. 1996, ApJ, 472, 783

Endal, A. S. & Sofia, S. 1976, ApJ, 210, 184

——1978, ApJ, 220, 279

Henyey, L. & L'Ecuyer, J. 1969, ApJ, 156, 549

Hernanz, M., Isern, J., Canal, R., Labay, J., & Mochkovitch, R. 1988, ApJ, 324, 331

Hoyle,F. & Fowler, W.A. 1960, ApJ, 132, 565

Huebner, W. F., Merts, A. L., Magee, Jr. M. H. & Argo, M. F. 1977, Los Alamos, Sci. Lab. Rep. LA-6760-M

Iben, I., Jr. 1982, ApJ, 259, 244

Iben, I., Jr. 1988, ApJ, 324, 355

Iben, I., Jr. & Tutukov, A. V. 1984, ApJS, 54, 335

Iben, I., Jr., Tutukov, A. V., & Fedorova, A. V. 1998, ApJ, 503, 344

Iben, I., Jr. & Tutukov, A. V., & Yungelson, L. R. 1997, ApJ, 475, 291

Isern, J., Labay, J., Hernanz, M., & Canal, R. 1983, ApJ, 273, 320

Itoh, N., Hayashi, H. & Kohyama, Y. 1993, ApJ, 418, 405

Kawai, Y., Saio, H, & Nomoto, K. 1987, ApJ, 315, 229

Kippenhan, R. & Thomas, H. C. 1970, in Stellar Rotation, Ed. Slettebak, Reidel, Dordrecht, p. 20

Koen, C., Orosz, J. A. & Wade, R. A. 1998, MNRAS, 300, 695

Limongi, M. & Tornambé, A. 1991, ApJ, 371, 317

Livio, M. 2000, in The greatest Explosions since the Big Bang: Supernovae and Gamma-Ray Bursts, Eds. M. Livio, N. Panagia & K. Sahu, in press

Ma, F. 2002, astro-ph/0202040

Maeder, A. & Meynet, G. 2000, ARA& A, 38, 143

Margenau, H. & Murphy, M. M. 1943, The Mathematics of Physics and Chemistry (D. Van Nostrand: Boston)

Mitake, S., Ichimaru, S. & Itoh, N. 1984, ApJ, 277, 375

Mochkovitch, R., Guerrero, J. & Segretain, L., 1997, in Thermonuclear Supernovae, Eds. P. Ruiz-Lapuente, R. Canal & J. Isern, Kluwer, Dordrecht, p. 187

Nomoto, K. 1982a, ApJ, 253, 798

Nomoto, K. 1982b, ApJ, 257, 780

Nomoto, K. & Iben, I., Jr. 1985, ApJ, 297, 531

Nomoto, K. & Sugimoto, D. 1977, PASJ, 29, 765

Ostriker, J. P. & Bodenheimer, P. 1968, ApJ, 151, 1089

Phillips, M. M. 1993, ApJL, 413, L105

Rasio, F. A. & Shapiro, S. L. 1995, ApJ, 438, 887

Saffer, R. A., Livio, M. & Yungelson, L. R. 1998, ApJ, 502, 394

Saio, H, & Nomoto, K. 1985, A& A, 150, L21

Saio, H, & Nomoto, K. 1998, ApJ, 500, 388

Salaris, M., Dominguez, I., Garcia-Berro, E., Hernanz, M. Isern, J. & Mochkovitch, R. 1997, ApJ, 486, 413

Shapiro, S. L. & Teukolsky, S. A. 1983, Black Holes, White Dwarfs and Neutron Stars, Wiley, New York

Shapiro, S. L. & Teukolsky, S. A. 1990, ApJL, 357, 17

Straniero, O. 1988, A& AS, 76, 157

Sugimoto, D. 1970 ApJ, 159, 619

Taam, R. E. 1980a, ApJ, 237, 142

Taam, R. E. 1980b, ApJ, 242, 749

Tassoul, J. L. 1978, Theory of Rotating Stars, Princeton Series in Astrophyiscs, Princeton University Press

Timmes, F. X., Woosley, S. E. & Taam, R. E. 1994, ApJ, 420, 348

Tutukov, A. V., & Yungelson, L. R. 1979, Acta Astr, 29, 665

Webbink, R. F. 1984, ApJ, 277, 355

Webbink, R. F., & Iben, I. Jr. 1988, in Faint Blue Stars, ed. A. G. Davis Philip, D. S. Hayes, and J. W. Liebert (Schenectady: L. Davis), p. 445, 1988.

Whelan, J. C. & Iben, I., Jr. 1973, ApJ, 186, 1007

This manuscript was prepared with the AAS LaTeX macros v4.0.

Table 1. Results of experiments with standard conditions on a $0.8M_\odot$ CO WD accreting at different accretion rates. $\dot{M}$ is the accretion rate (in $M_\odot$ yr^{-1}), $M_{\rm f}$ (in $M_\odot$) is the total mass at carbon ignition, $M_{\rm ig}$ is the mass coordinate where carbon burning is ignited (in $M_\odot$), $T_{\rm ig}$ (in K) and $\rho_{\rm ig}$ (in g cm^{-3}) are, respectively, the temperature and the density at the ignition point.

$\dot{M}$	$M_{\rm f}$	$M_{\rm ig}$	$\log(T_{\rm ig})$	$\log(\rho_{\rm ig})$
10^{-5}	1.037	0.899	8.785	5.977
5×10^{-6}	1.193	1.134	8.773	6.242
3×10^{-6}	1.315	1.297	8.772	6.390
2×10^{-6}	1.383	0.000[a)]	8.295	9.565
10^{-6}	1.380	0.098	8.381	9.371
5×10^{-7}	1.375	0.000	8.348	9.392
10^{-7}	1.380	0.000	8.287	9.505
5×10^{-8}	1.383	0.000	8.237	9.576
10^{-8}	1.395	0.000	8.101	9.705

[a)]During the subsequent evolution of this model, the mass coordinate where the nuclear energy production is maximum jumps to the point $M = 1.375\ M_\odot$ just below the surface.

Fig. 1.— Chemical profiles of ^{12}C and ^{16}O in a 0.8 $M_\odot$ model at the beginning of the cooling sequence as obtained by evolving a pure He star (*panel a*) and as it becomes after the re-homogenization made according to Salaris et al. (1997) (*panel b*) (see text).

Fig. 2.— Time evolution of the thermal diffusion time scale (solid lines) and of the compressional heating time scale (dashed lines) for all of the computed models as listed in Table 1.

Fig. 3.— Time evolution of the central temperature (solid line), the thermal diffusion time scale (dashed line), the mass coordinate where the maximum temperature is located (long dashed line) for the model with $\dot{M} = 10^{-8}$ $M_\odot$ yr^{-1} (see text). All the quantities have been normalized to their maximum value.

Fig. 4.— Evolution of the temperature and of ratios of several time scales in the interior of a model accreting at the rate 10^{-5} $M_\odot$ yr^{-1}. Here, $\tau_{\rm diff,loc}$ is a local diffusion time scale, $\tau_{\rm comp}$ is a local compressional time scale, and $\tau_{\rm evo}$ is the time elapsed from the beginning of the accretion experiment.

Fig. 5.— Same as Fig. 4, but for $\dot{M} = 10^{-8}$ $M_\odot$ yr^{-1}.

Fig. 6.— Evolution in the HR diagram of all of the computed models listed in Table 1 (see text). Attached to each line is the corresponding value of $\dot{M}$ (in $M_\odot$ yr^{-1}).

Fig. 7.— Time evolution of the surface radius for all of the models listed in Table 1 (see text). Attached to each line the corresponding value of $\dot{M}$ (in $M_\odot$ yr^{-1}).

Fig. 8.— Evolution in the $\rho - T$ plane of the center of the 0.8 $M_\odot$ CO WD accreting matter at various $\dot{M}$, as labeled inside the figure (in $M_\odot$ yr^{-1}) (see Table 1). The long-dashed curve labeled " $\varepsilon_\nu = \varepsilon_{cc}$ " is the ignition curve.

Fig. 9.— Temperature profiles for several selected structures during the accretion process for different values of the accretion rate, as labeled inside each panel.

Fig. 10.— Density profiles for the same models as in Fig. 9.

Fig. 11.— Profiles in the $\rho - T$ plane of models which have attained the physical conditions suitable for carbon ignition as a consequence of mass accretion at different $\dot{M}$, as labeled inside the figure (in units of $M_\odot$ yr^{-1}).

Fig. 12.— Initial value of the thermal diffusion time scale $\tau_{\rm diff}$ (in yr) as a function of the initial angular velocity (in units of $\omega_{\rm crit,0}$).

Fig. 13.— Time evolution of the surface radius for models rotating with different initial angular velocities as labeled inside the figure (in units of $\omega_{\rm crit,0}$). Each panel refers to a different value of the accretion rate as labeled. For comparison the evolution of the standard model without rotation (dashed line) is also shown.

Fig. 14.— Evolution of the diffusion time scale in the outer zone (*panel a*), the surface temperature (*panel b*), and the total radius (*panel c*) of the model with $\dot{M} = 10^{-8}$ $M_\odot$ yr^{-1} and $\omega_0 = 0.5\omega_{\rm crit,0}$. In *panel d*, the evolution of the white dwarf angular velocity (lower curve) is compared with that of the critical angular velocity at the surface (upper curve).

Fig. 15.— The region in the parameter space $\dot{M} - \omega_0$ (shaded zone) for which the rotating models accreting CO-rich matter become gravitationally unbound when the total mass of the WD approaches 1.4 $M_\odot$ (see text).

Fig. 16.— The same as in Fig. 14, but for the case $\dot{M} = 10^{-8}$ $M_\odot$ yr^{-1} and $\omega_0 = 0.1\omega_{\rm crit,0}$.

Fig. 17.— Temperature profiles of selected structures during the evolution of the rotating model with $\omega_0 = 0.1\omega_{\rm crit,0}$ and accreting matter at $\dot{M} = 10^{-8}$ $M_\odot$ yr^{-1}. The labels attached to each line provide the time elapsed from the beginning of the accretion process.

Fig. 18.— Evolution of the surface radius for models accreting CO-rich matter at $\dot{M} = 10^{-7} M_{\odot}$ yr^{-1} with different values of the initial angular velocity computed by assuming that the accreted matter does (dashed lines) or does not deposit (solid lines) angular momentum (see text).

Fig. 19.— The same as in Fig. 15, but for rotating models which accrete CO-rich matter at rest (see text).

Fig. 20.— Temperature profiles for some selected structures during the braking stage of a rotating $\sim 1.42\ M_{\odot}$ CO WD. The braking time scale has been set equal to 10^7 yr (see text).

Fig. 21.— Temperature profiles for some selected structures during the braking stage of a rotating $\sim 1.42\ M_{\odot}$ CO WD. The braking time scale has been set equal to 10^3 yr (see text).

Fig. 22.— Evolution in the $\rho - T$ plane of the center of models accreting CO-rich matter at $\dot{M} = 10^{-8}\ M_{\odot}$ yr^{-1}. The dashed line describes the evolution of the standard model ($\omega = 0$), whereas the solid lines describe the evolution of two rotating models with $\omega_0 = 0.1\omega_{\rm crit,0}$ and two different GWR-braking times, one with $\tau = 10^3$ yr, the other with $\tau = 10^7$ yr (see text).

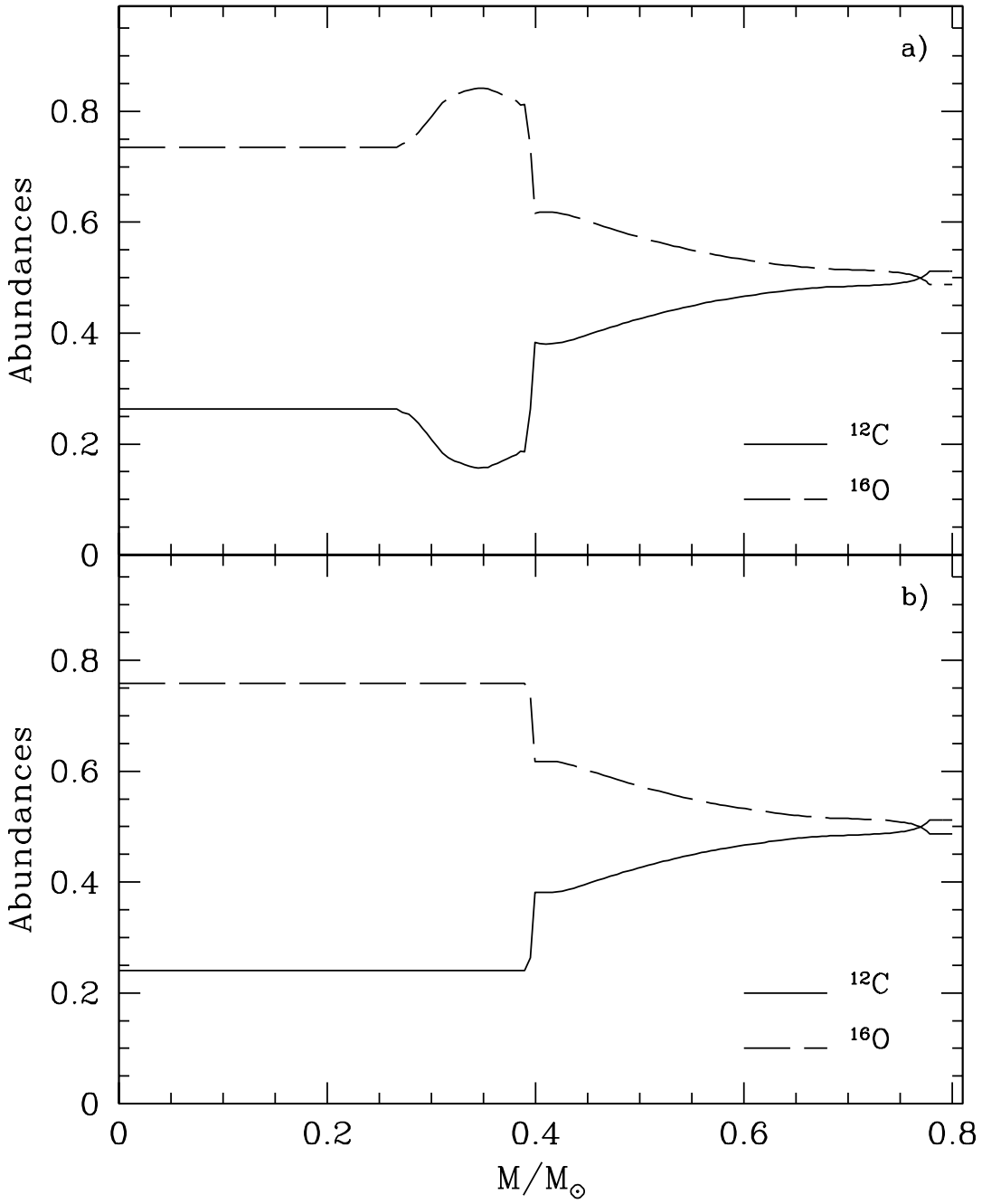
a)
b)
Abundances
0
0.2
0.4
0.6
0.8
^{12}C
^{16}O
0
0.2
0.4
0.6
0.8
$M/M_\odot$

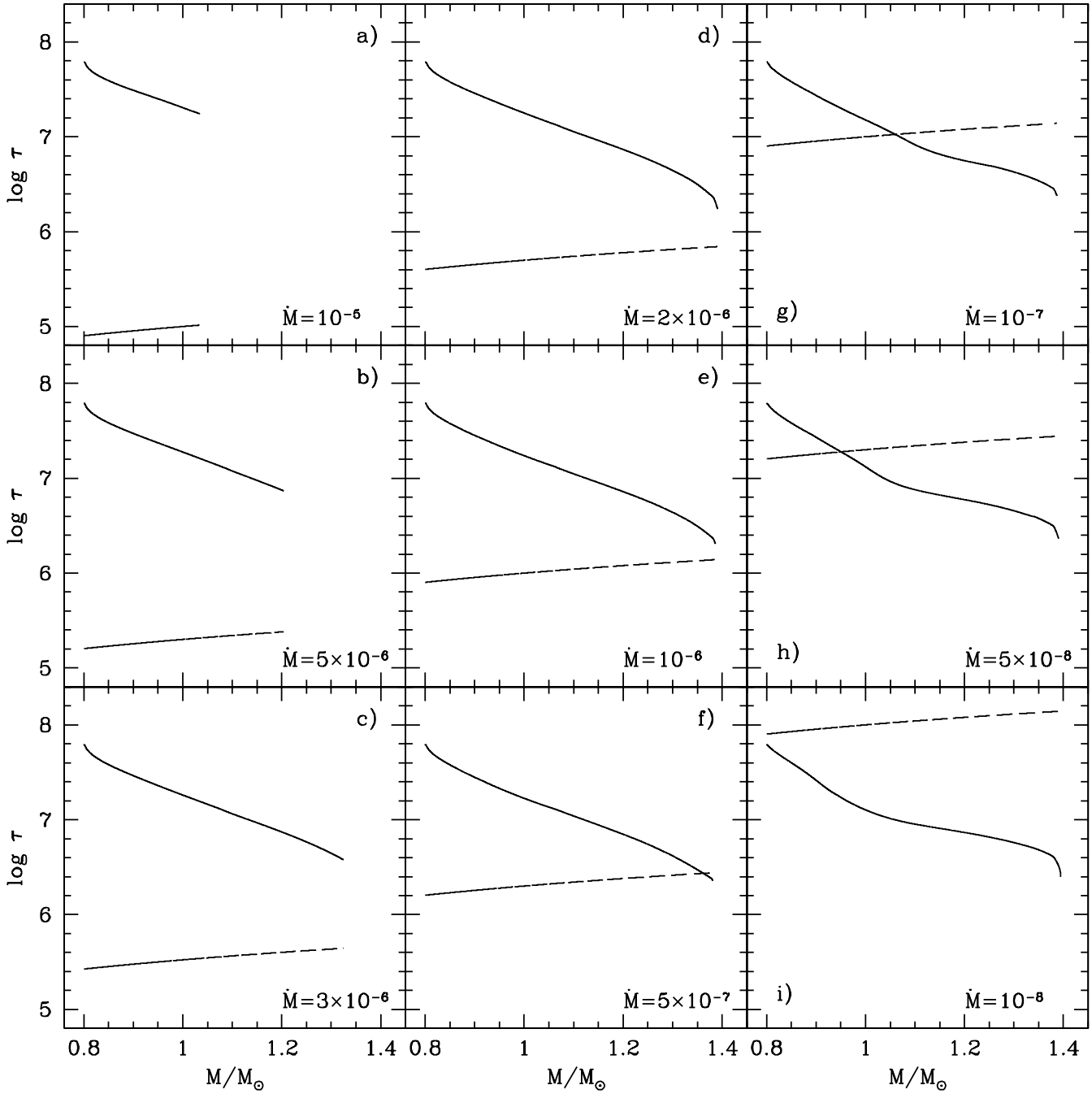
a)
b)
c)
d)
e)
f)
g)
h)
i)
$\dot{M}=10^{-5}$
$\dot{M}=5\times10^{-6}$
$\dot{M}=3\times10^{-6}$
$\dot{M}=2\times10^{-6}$
$\dot{M}=10^{-6}$
$\dot{M}=5\times10^{-7}$
$\dot{M}=10^{-7}$
$\dot{M}=5\times10^{-8}$
$\dot{M}=10^{-8}$
log τ
$M/M_\odot$
5
6
7
8
0.8
1
1.2
1.4

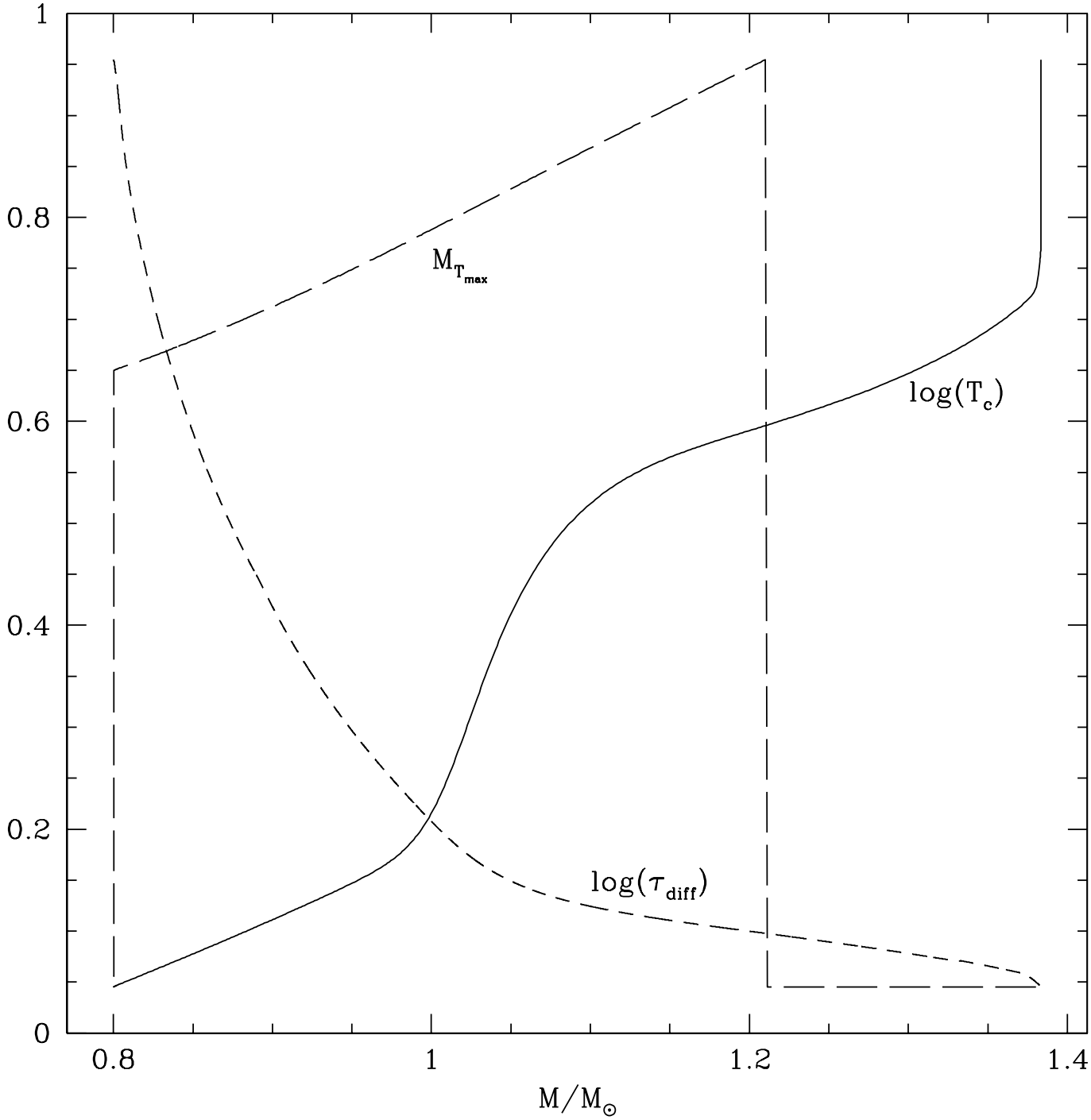
1
0.8
0.6
0.4
0.2
0
0.8
1
1.2
1.4
$M/M_\odot$
$M_{T_{max}}$
$\log(T_c)$
$\log(\tau_{diff})$

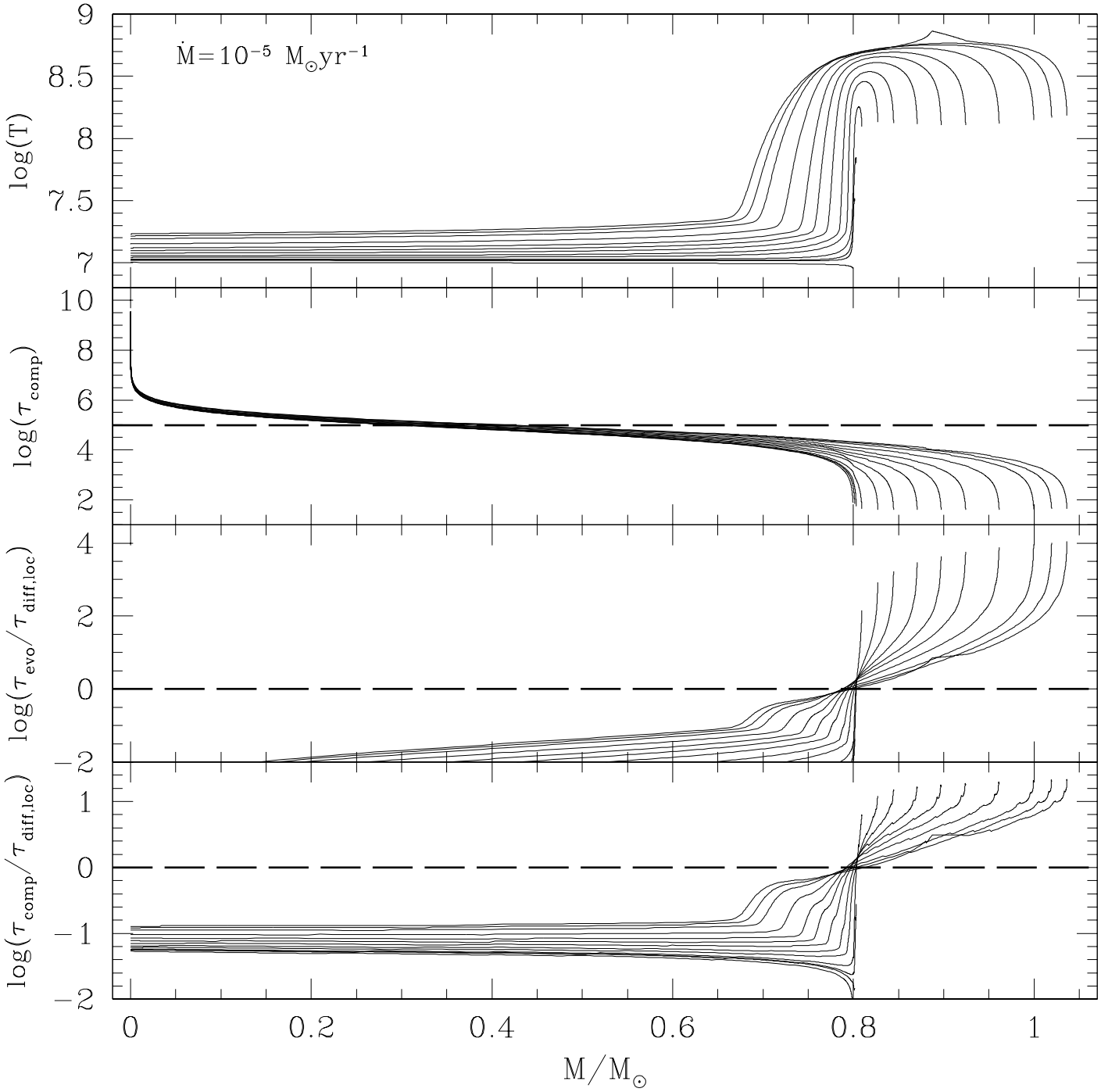
$\dot{M}=10^{-5}$ $M_\odot yr^{-1}$
log(T)
$\log(\tau_{comp})$
$\log(\tau_{evo}/\tau_{diff,loc})$
$\log(\tau_{comp}/\tau_{diff,loc})$
$M/M_\odot$

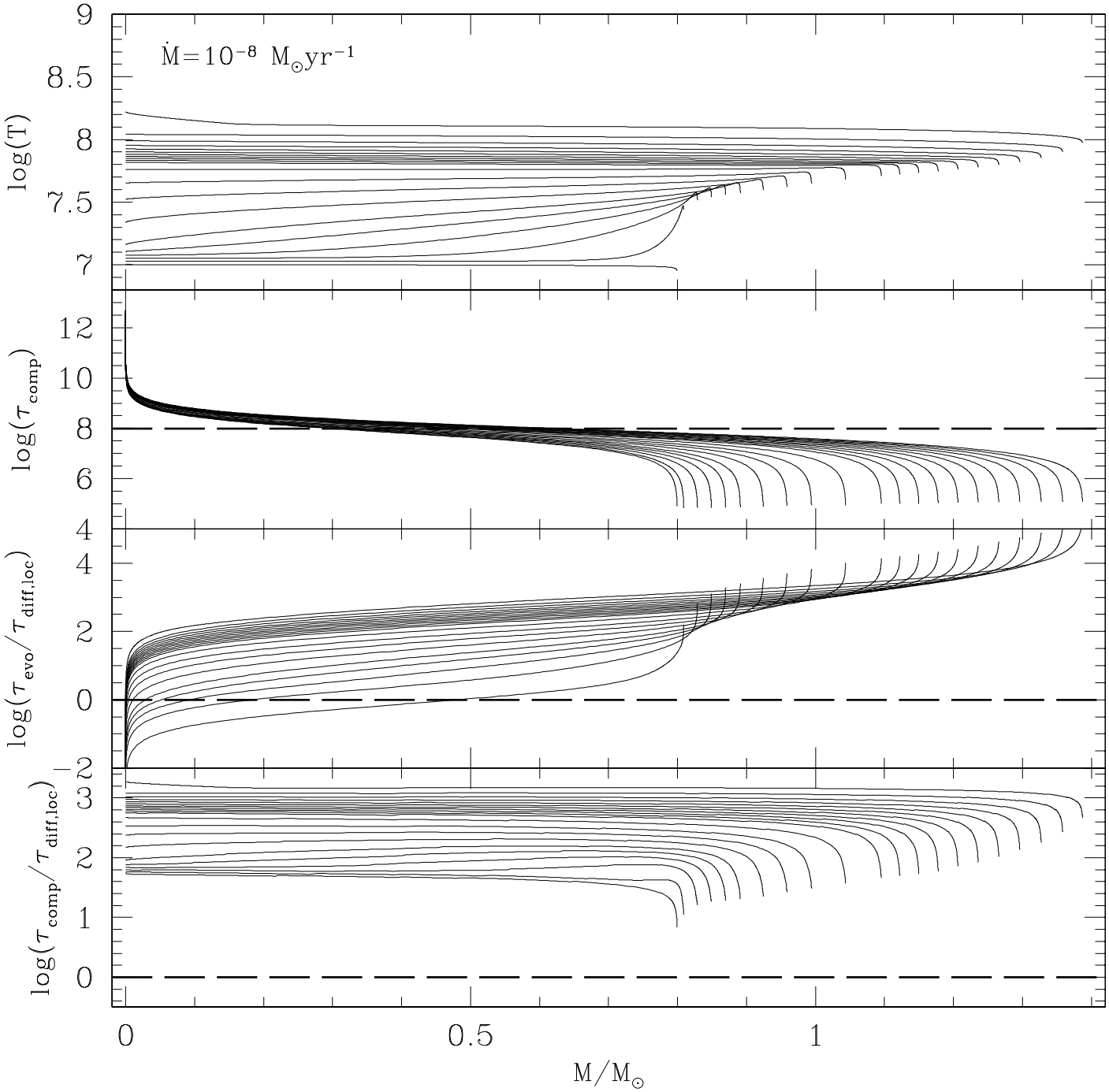
$\dot{M}=10^{-8}$ $M_\odot yr^{-1}$
log(T)
$\log(\tau_{comp})$
$\log(\tau_{evo}/\tau_{diff,loc})$
$\log(\tau_{comp}/\tau_{diff,loc})$
$M/M_\odot$

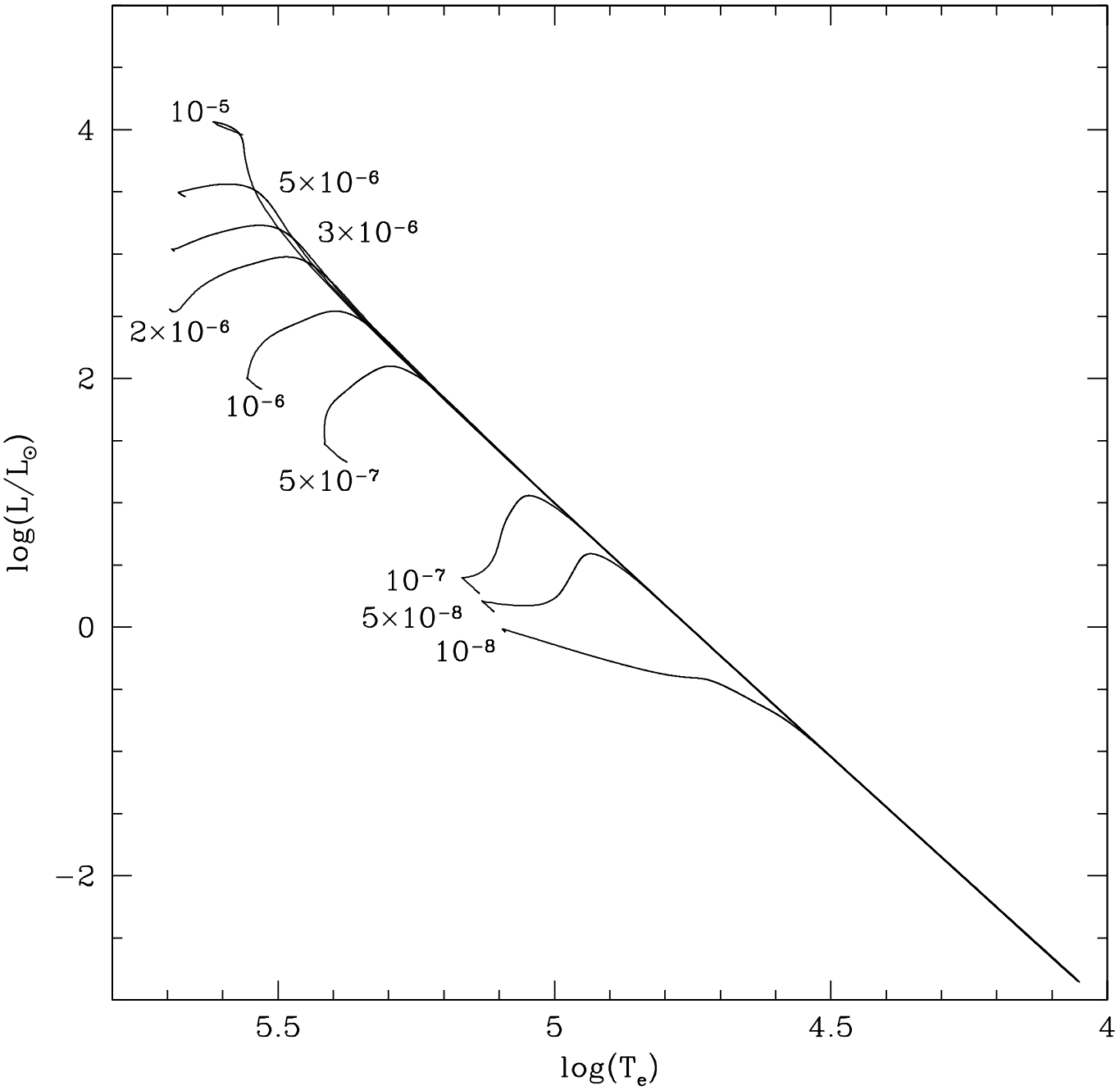
10^{-5}
5×10^{-6}
3×10^{-6}
2×10^{-6}
10^{-6}
5×10^{-7}
10^{-7}
5×10^{-8}
10^{-8}
4
2
0
−2
5.5
5
4.5
4
$\log(L/L_\odot)$
$\log(T_e)$

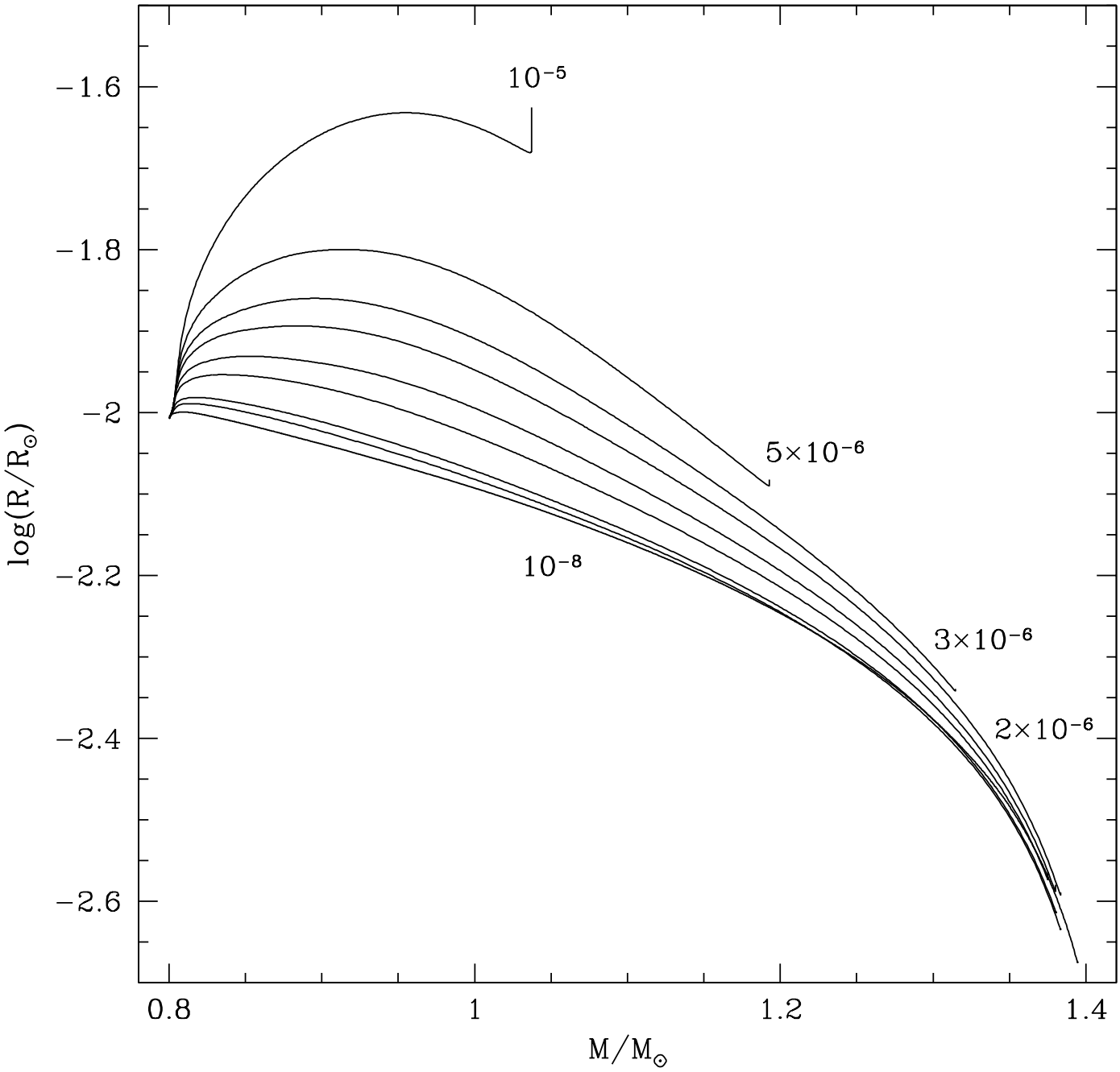
10^{-5}
5×10^{-6}
3×10^{-6}
2×10^{-6}
10^{-8}
−1.6
−1.8
−2
−2.2
−2.4
−2.6
0.8
1
1.2
1.4
$\log(R/R_\odot)$
$M/M_\odot$

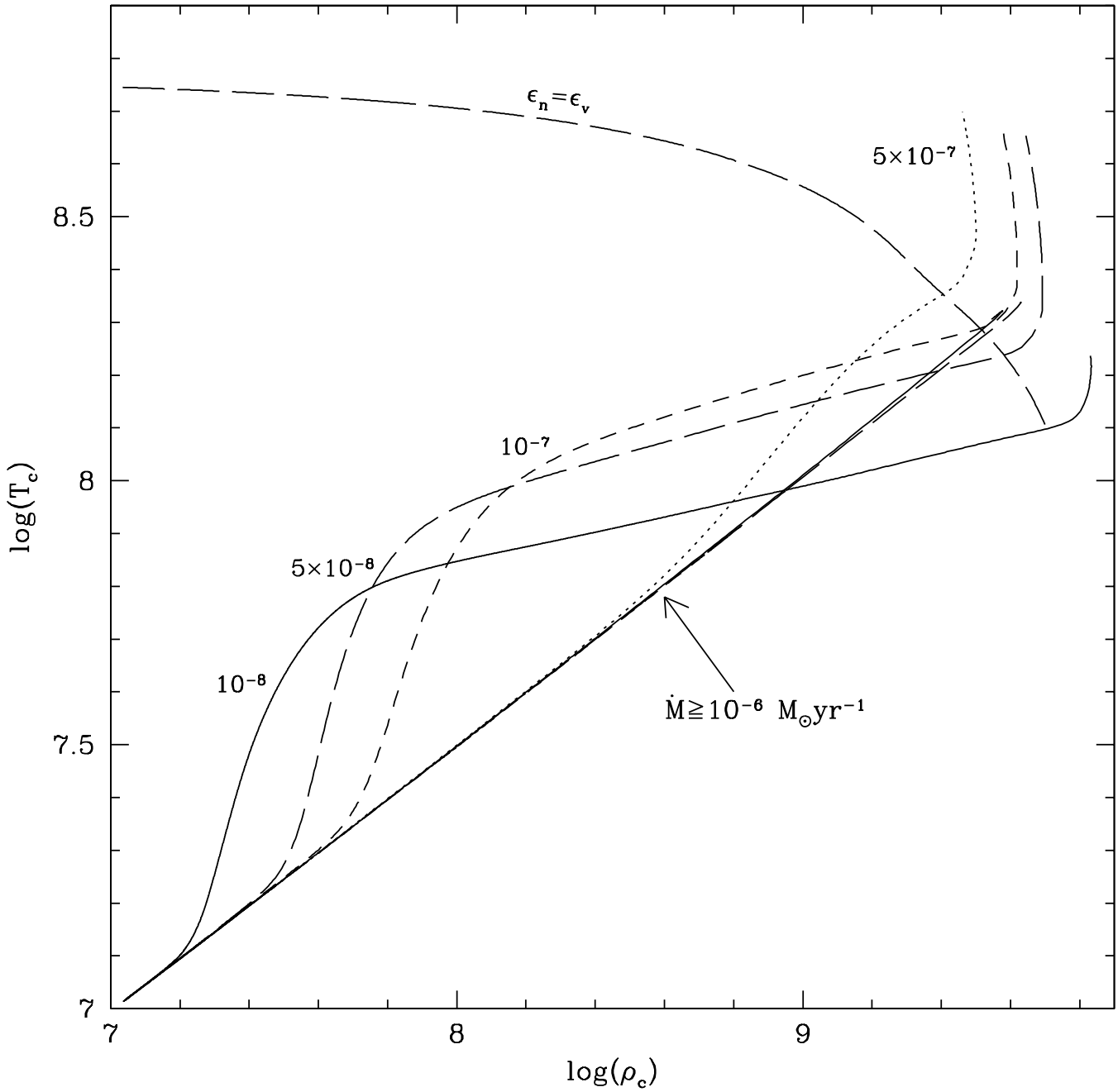
$\epsilon_n = \epsilon_\nu$
5×10^{-7}
10^{-7}
5×10^{-8}
10^{-8}
$\dot{M} \geqq 10^{-6}\ M_\odot yr^{-1}$
8.5
8
7.5
7
7
8
9
$\log(T_c)$
$\log(\rho_c)$

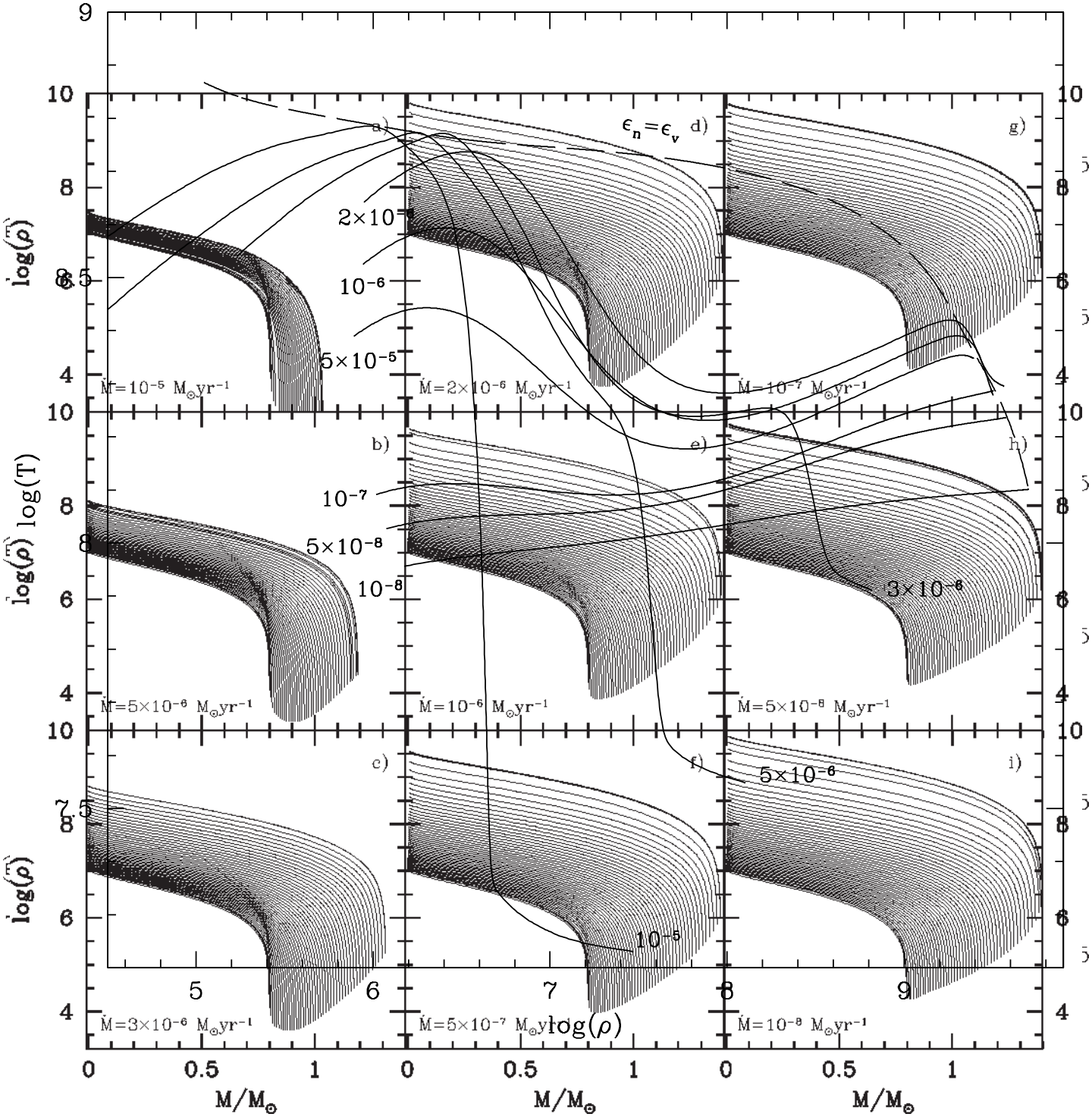
a)
b)
c)
d)
e)
f)
g)
h)
i)
$\epsilon_n = \epsilon_\nu$
2×10^{-6}
10^{-6}
5×10^{-5}
10^{-7}
5×10^{-8}
10^{-8}
3×10^{-6}
5×10^{-6}
10^{-5}
$\dot{M}=10^{-5}$ $M_\odot yr^{-1}$
$\dot{M}=2\times10^{-6}$ $M_\odot yr^{-1}$
$\dot{M}=10^{-7}$ $M_\odot yr^{-1}$
$\dot{M}=5\times10^{-6}$ $M_\odot yr^{-1}$
$\dot{M}=10^{-6}$ $M_\odot yr^{-1}$
$\dot{M}=5\times10^{-8}$ $M_\odot yr^{-1}$
$\dot{M}=3\times10^{-6}$ $M_\odot yr^{-1}$
$\dot{M}=5\times10^{-7}$ $M_\odot yr^{-1}$
$\dot{M}=10^{-8}$ $M_\odot yr^{-1}$
$\log(\rho)$
$\log(T)$
$M/M_\odot$

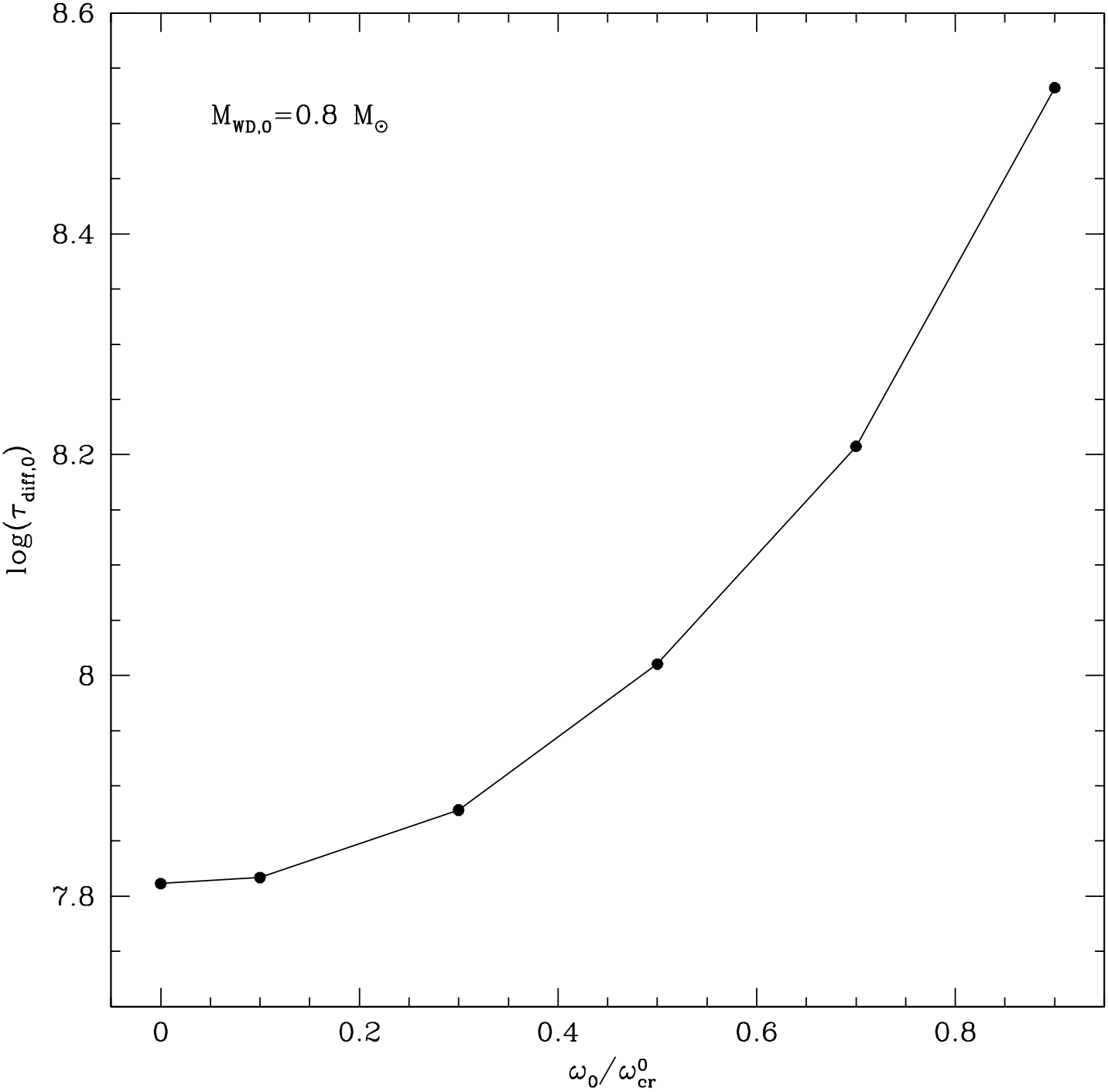
$M_{WD,0}$=0.8 $M_\odot$
8.6
8.4
8.2
8
7.8
$\log(\tau_{diff,0})$
0
0.2
0.4
0.6
0.8
ω_0/ω^0_{cr}

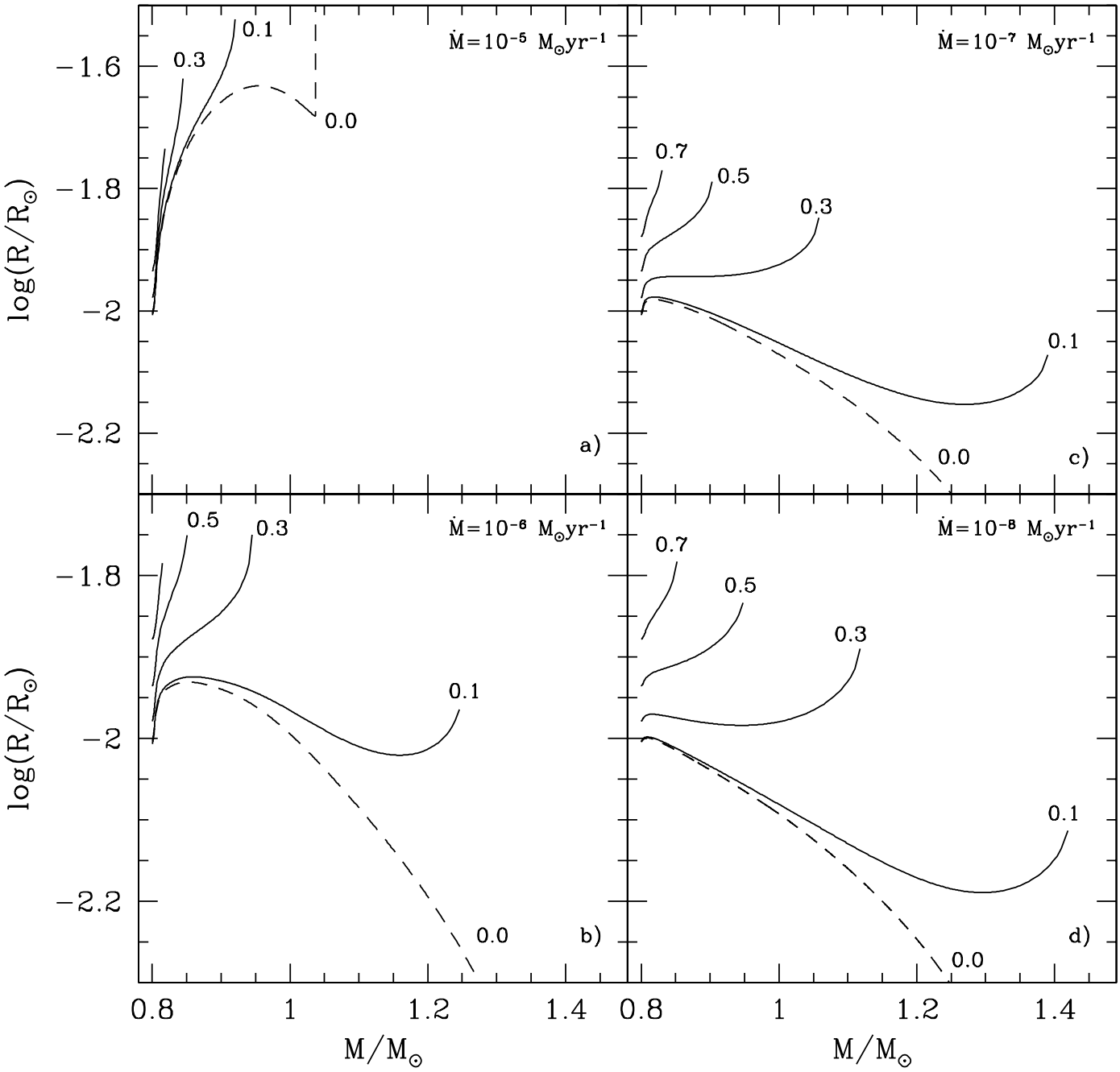
$\dot{M}=10^{-5}$ $M_\odot yr^{-1}$
$\dot{M}=10^{-7}$ $M_\odot yr^{-1}$
$\dot{M}=10^{-6}$ $M_\odot yr^{-1}$
$\dot{M}=10^{-8}$ $M_\odot yr^{-1}$
a)
b)
c)
d)
0.0
0.1
0.3
0.5
0.7
$\log(R/R_\odot)$
$M/M_\odot$
−1.6
−1.8
−2
−2.2
0.8
1
1.2
1.4

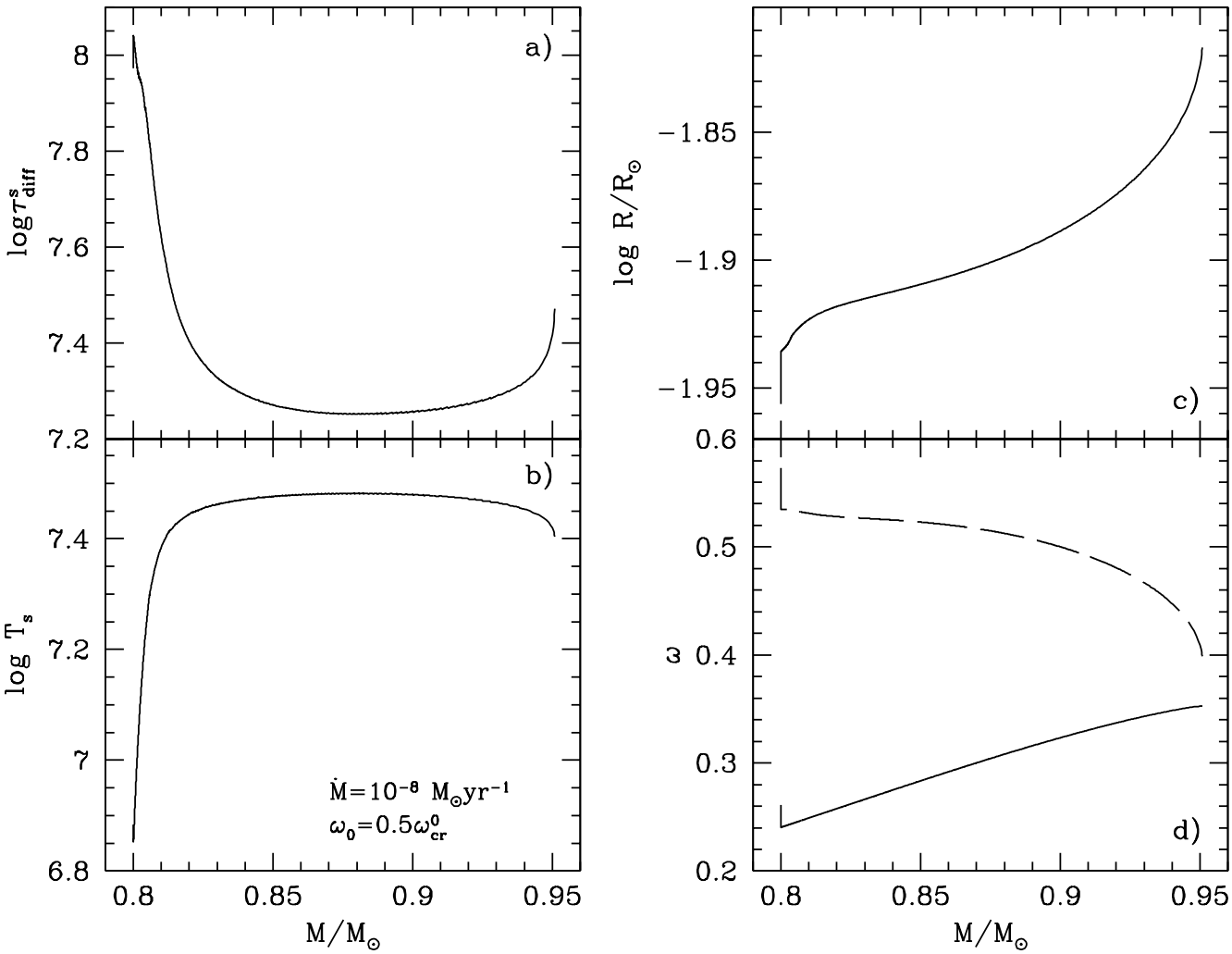
a)
b)
c)
d)
$\log \tau^s_{diff}$
$\log T_s$
$\log R/R_\odot$
$\mathfrak{z}$
$\dot{M}=10^{-8}\ M_\odot yr^{-1}$
$\omega_0=0.5\omega^0_{cr}$
$M/M_\odot$
$M/M_\odot$

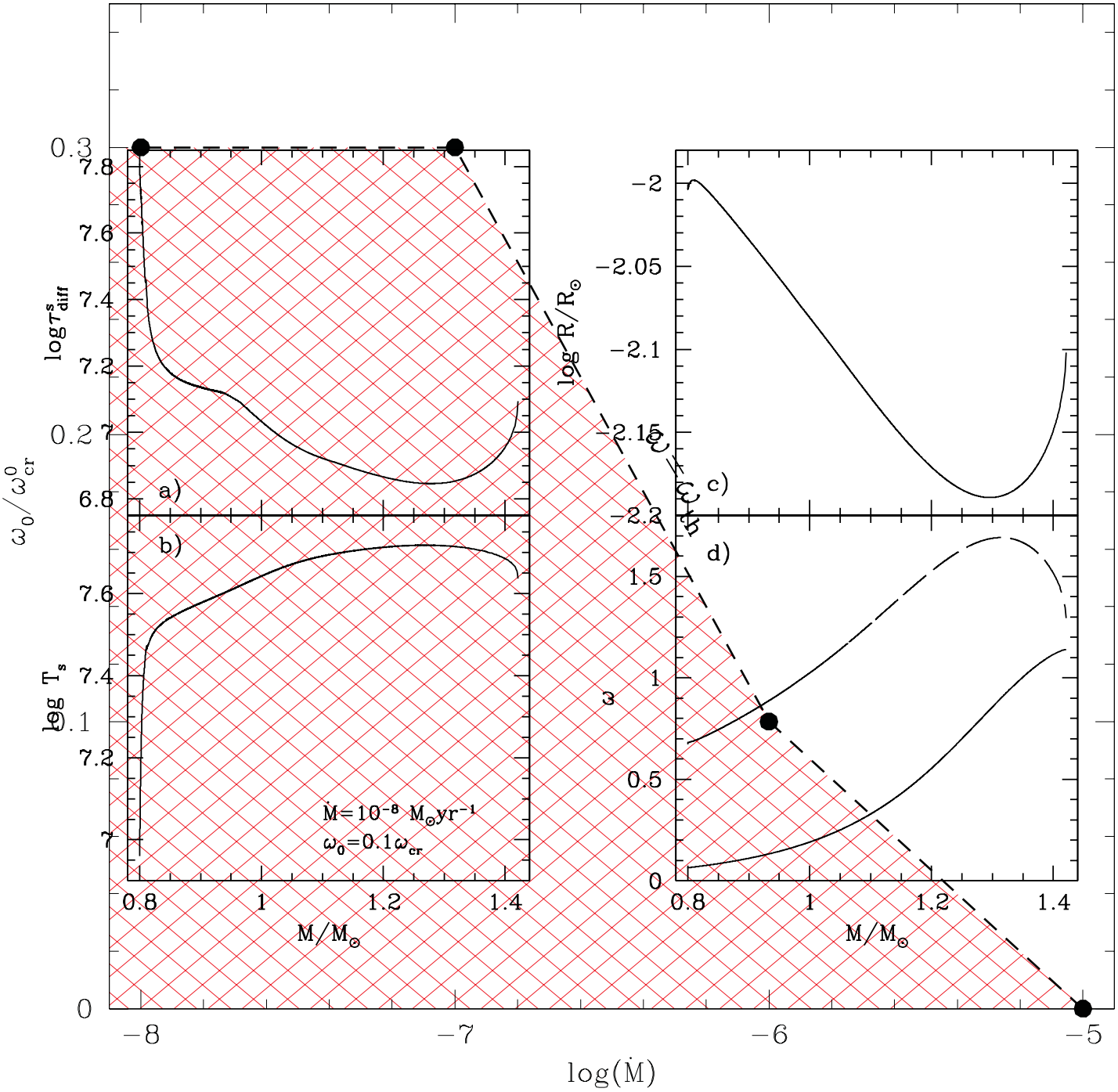
a)
b)
c)
d)
$\log \tau^s_{diff}$
$\log T_s$
$\log R/R_\odot$
ω_0/ω^0_{cr}
$\dot{M}=10^{-8}\ M_\odot yr^{-1}$
$\omega_0=0.1\omega_{cr}$
$M/M_\odot$
$\log(\dot{M})$

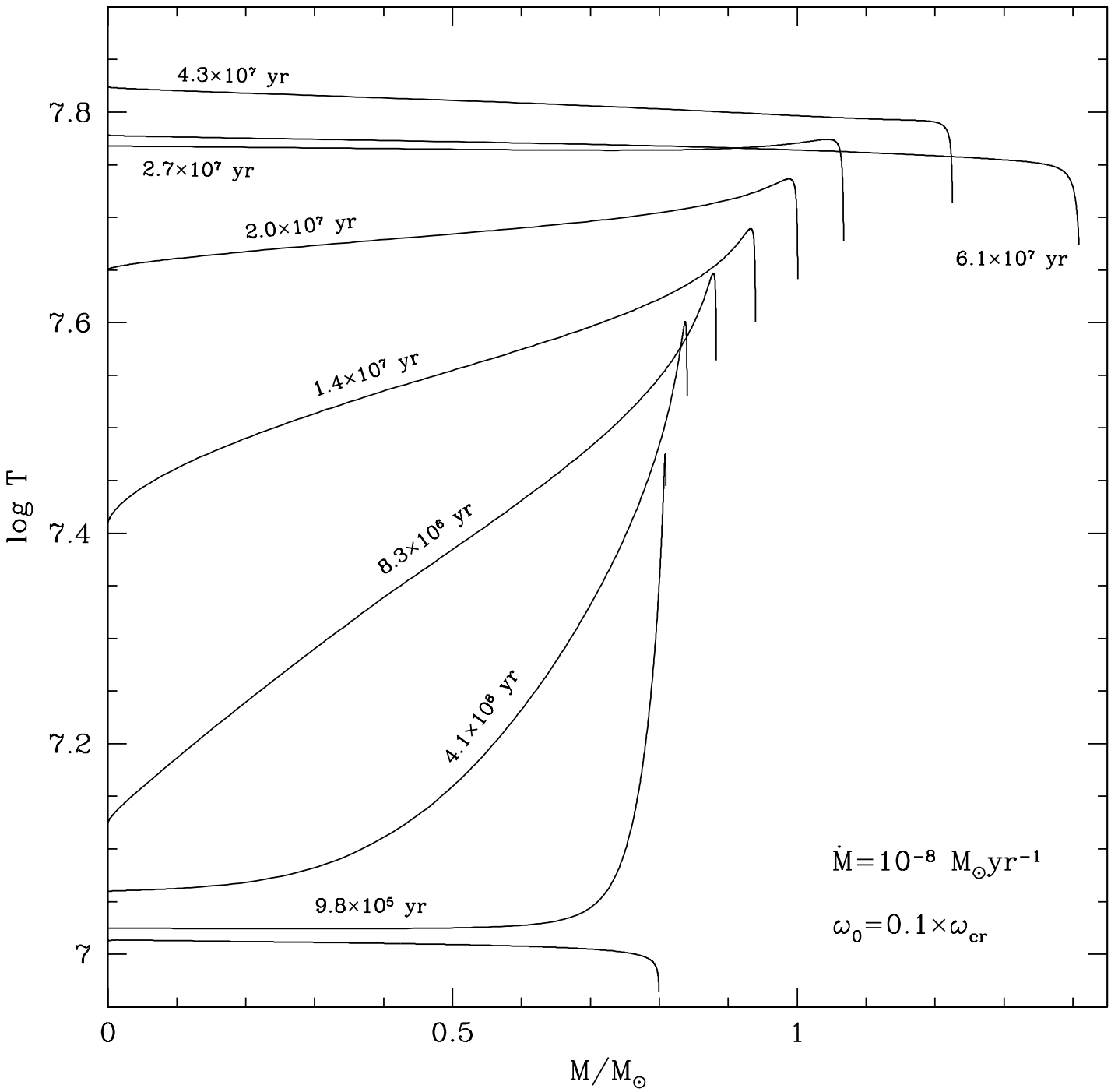
4.3×10⁷ yr
2.7×10⁷ yr
2.0×10⁷ yr
6.1×10⁷ yr
1.4×10⁷ yr
8.3×10⁶ yr
4.1×10⁶ yr
9.8×10⁵ yr
Ṁ=10⁻⁸ M⊙yr⁻¹
ω0=0.1×ωcr
log T
7.8
7.6
7.4
7.2
7
0
0.5
1
M/M⊙

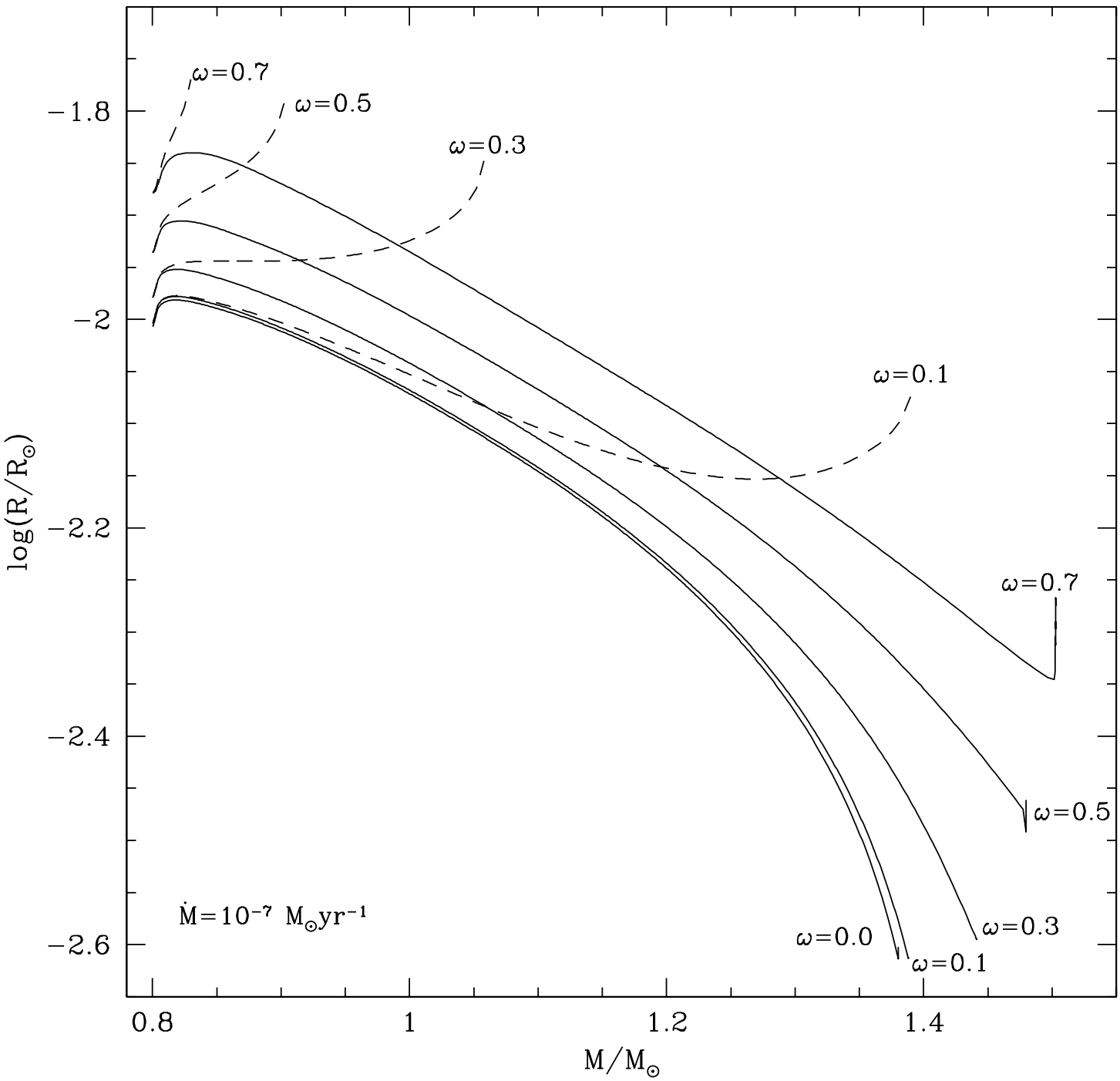
ω=0.7
ω=0.5
ω=0.3
ω=0.1
ω=0.7
ω=0.5
ω=0.3
ω=0.1
ω=0.0
Ṁ=10⁻⁷ M⊙yr⁻¹
−1.8
−2
−2.2
−2.4
−2.6
0.8
1
1.2
1.4
log(R/R⊙)
M/M⊙

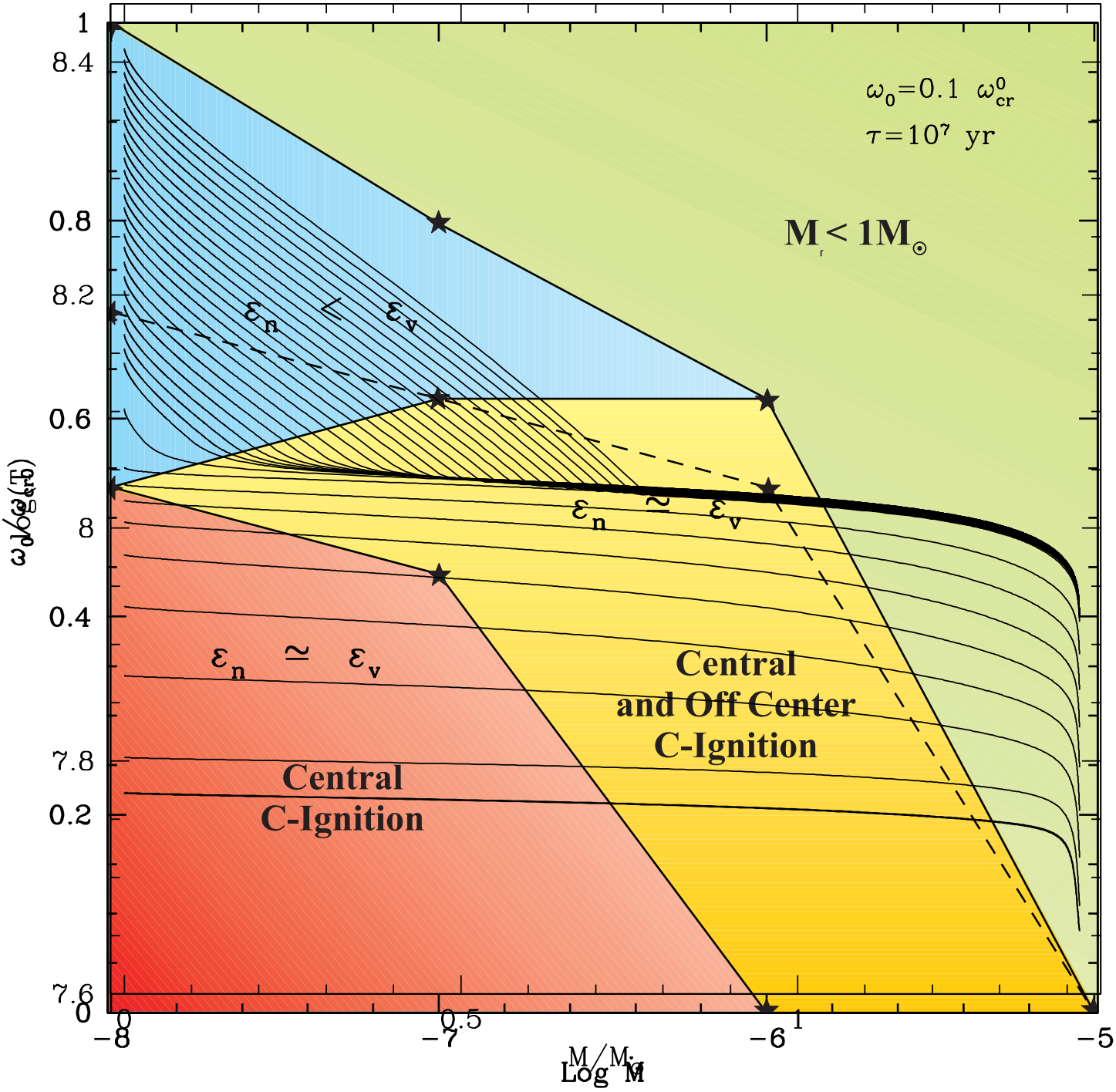
$\omega_0 = 0.1\ \omega_{cr}^0$
$\tau = 10^7$ yr
$M_r < 1 M_\odot$
$\varepsilon_n < \varepsilon_v$
$\varepsilon_n \simeq \varepsilon_v$
$\varepsilon_n \simeq \varepsilon_v$
Central and Off Center C-Ignition
Central C-Ignition
$\omega_0/\omega_{cr}(T_b)$
Log $M_r/M_\odot$
1
8.4
0.8
8.2
0.6
8
0.4
7.8
0.2
7.6
0
0.5
1
−8
−7
−6
−5

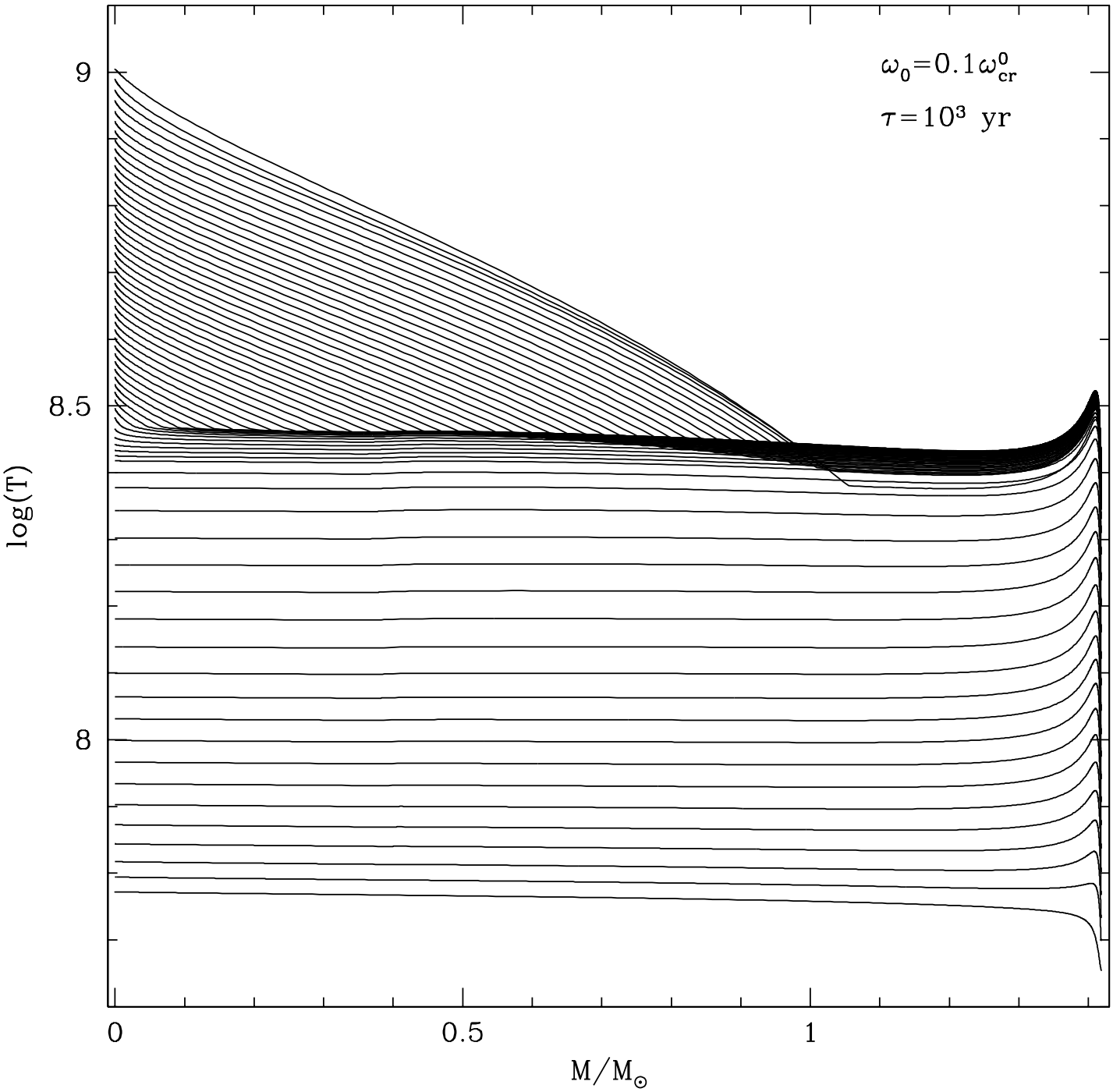
$\omega_0 = 0.1\omega^0_{cr}$
$\tau = 10^3$ yr
9
8.5
8
log(T)
0
0.5
1
$M/M_\odot$

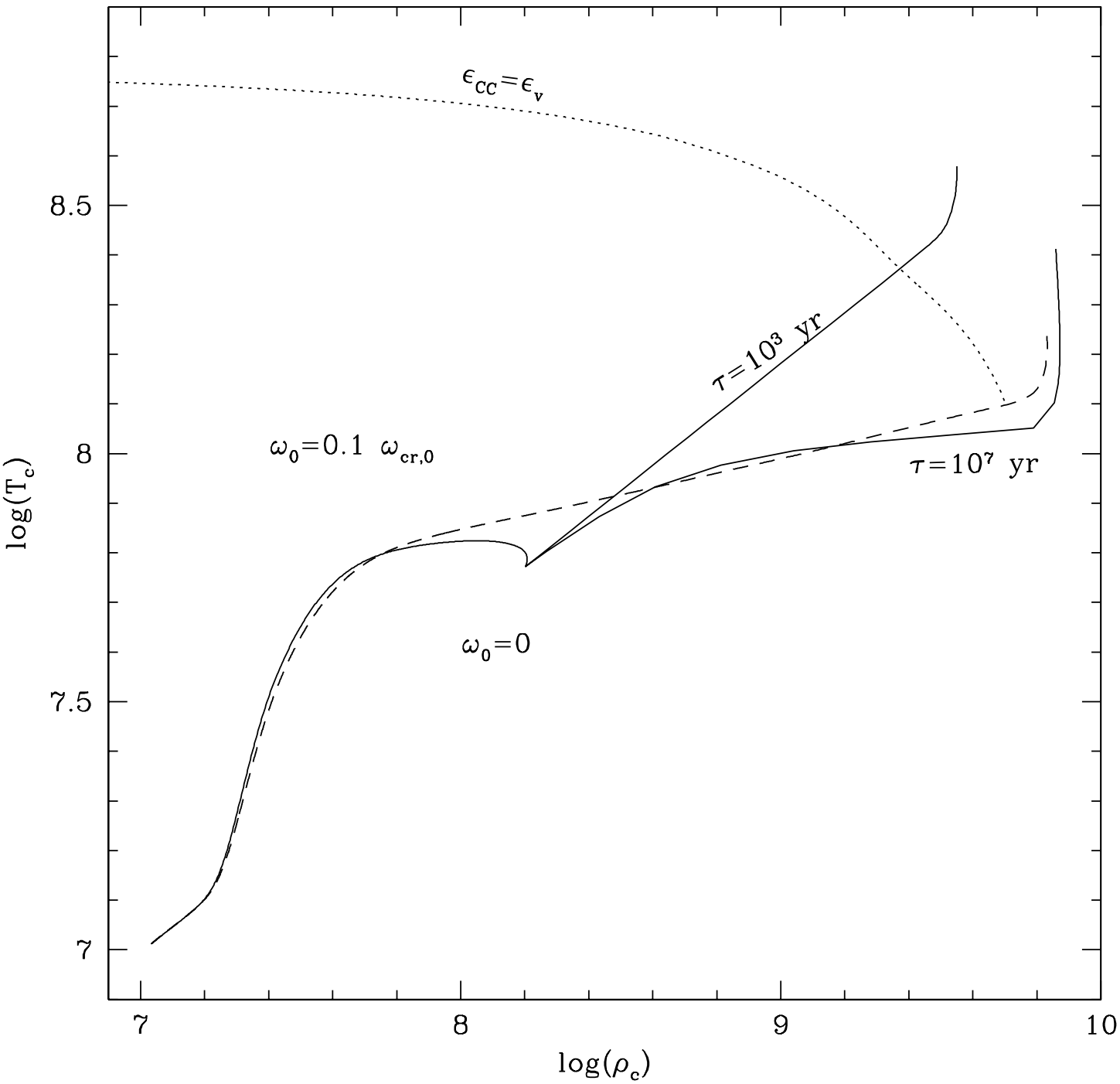
$\epsilon_{CC}=\epsilon_\nu$
$\tau=10^3$ yr
$\omega_0=0.1\ \omega_{cr,0}$
$\tau=10^7$ yr
$\omega_0=0$
8.5
8
7.5
7
7
8
9
10
$\log(T_c)$
$\log(\rho_c)$